The influence of earthquake gates on surface rupture length

A.M. Rodriguez Padilla [1,2*], M.E. Oskin[1], E.E. Brodsky[3], K. Dascher-Cousineau[4], V. Herrera[5], S. White[6,7]

[1] Department of Earth and Planetary Sciences, University of California, Davis

[2] Now at Division of Geological and Planetary Sciences, California Institute of Technology

[3] Department of Earth and Planetary Sciences, University of California, Santa Cruz

[4] Department of Earth and Planetary Sciences, University of California, Berkeley

[5] Department of Earth and Environmental Sciences, San Diego State University

[6] Geology Department, Pasadena City College

[7] Now at Department of Earth, Planetary, and Space Sciences, University of California, Los Angeles

*Corresponding author: Alba M. Rodriguez Padilla (alba@caltech.edu, amrodriguezpadilla@gmail.com)

Key Points:

- We map step-overs, bends, gaps, splays, and strands from 31 strike-slip surface ruptures at 1:50,000 scale and investigate their potential as earthquake gates.
- Most step-overs wider than 1.2 km and bends with angles >30° consistently halt propagating ruptures, suggesting surficial complexity extends to depth.
- Our findings support that earthquake gates limit the size of large events.

Abstract

Propagating earthquakes must overcome geometrical complexity on fault networks to grow into large, surface rupturing events. We map step-overs, bends, gaps, splays, and strands of length scales ~100-500 meters from the surface ruptures of 31 strike-slip earthquakes, recording whether ruptures propagated past the feature. We find that step-overs and bends can arrest rupture and develop a statistical model for passing probability as a function of geometry for each group. Step-overs wider than 1.2 km, single bends larger than 32°, and double bends larger than 38° are breached by rupture half of the time. ~20% of the ruptures terminate on straight segments. We examine how the distribution of earthquake gates influences surface rupture length, inferring an exponential relationship between rupture length and event probability for a given fault. Our findings support that earthquake gates limit the size of large events and help discriminate between different proposed models of rupture propagation.

Plain Language Summary

Zones of geometrical complexity along faults can behave as barriers or earthquake gates that sometimes halt propagating earthquakes. We map five types of geometrical complexities from historical surface rupture maps and regional fault maps: step-overs, bends, gaps, splays, and strands at 1:50,000 scale, corresponding to features >100-500 m in length. This is a finer scale than previous studies, which focused on kilometer-scale zones of geometrical complexity. We classify each mapped zone of geometrical complexity as breached (earthquake propagated past) or unbreached (earthquake halted) and measure the width of step-overs and strands, the length of gaps, and the angle of splays and bends. Based on these measurements, we model the probability that each feature will be breached given its geometry. Step-overs wider than 1.2 km, single bends larger than 32°, and double bends larger than 38° are breached by rupture half of the time. ~20% of the ruptures terminate on straight segments. Using our probabilities, we show that the presence and geometry of earthquake gates in the 100-500 m length scale plays a first-order control on the low likelihood of large surface rupturing earthquakes.

Introduction

Earthquake surface ruptures are composed of fault segments bound by zones of geometrical complexity (e.g., Wesnousky, 2006; Manighetti et al., 2007; Klinger, 2010; Perrin et al., 2016; Hamling et al., 2017). These zones of geometrical complexity can act as earthquake gates where the probability of rupture propagation is conditional on prior earthquake history, rupture dynamics, material properties, and the stress conditions on neighboring fault segments. For earthquakes on vertically dipping strike-slip faults, where the thickness of the seismogenic zone limits down-dip rupture propagation, geometrical complexities have been proposed to exert an important control on rupture length, and thus magnitude (e.g., Wesnousky, 2006).

Historical earthquake rupture maps provide tests for geometrical controls on rupture propagation that serve as validation for rupture simulator forecasts and dynamic rupture models (e.g., Lettis et al., 2002; Wesnousky, 2006, 2008; Biasi and Wesnousky, 2016, 2017, 2021). Most previous studies relied on simplified rupture maps, limiting the minimum size of earthquake gates considered to kilometer-scale. This scale is practical for hazard applications, as it is comparable to the resolution of complexity on regional fault maps and is commensurable with model discretization in rupture simulators (Biasi and Wesnousky, 2021; Milner et al., 2022).

Though limited in potential for prospective hazard assessment, observations suggest that finer scale geometrical complexity can also exhibit earthquake gate behavior. For example, the 2014 Napa earthquake terminated in a 750-meter-wide step-over, too small to be included in most previous studies. With new surface rupture maps from recent events, concurrent with ongoing efforts to standardize past rupture maps (e.g., Sarmiento et al., 2021; Nurminen et al., 2022) and improve regional fault maps, it is now possible to consider whether finer scale geometrical complexity can act as an earthquake gate and how the distribution of this complexity influences the probability of rupture propagation and final event size.

In this study, we map geometrical complexities at 1:50,000 scale, which corresponds with features >100-500 meters in length scale, from 31 strike-slip surface rupture maps in the unified Fault Displacement Hazard Initiative (FDHI) database (Sarmiento et al., 2021) and their corresponding regional fault maps (see supplementary methods). We consider five types of geometrical complexity: step-overs, bends, splays, gaps, and strands (Figure 1). Step-overs are spaces between neighboring, parallel, overlapping faults. Bends are locations where the fault changes strike. Bends may come in pairs (double bends) where the fault returns to its original

orientation. Step-overs and double bends may be classified as a restraining (net contraction) or releasing (net extension), but single bends cannot be classified as such without knowledge of rupture propagation direction. Gaps are spaces between coplanar faults, distinct from step-overs, where faults are not coplanar. Splays are locations where the fault branches. We also consider fault strands that are parallel to subparallel of the continuous, main rupture that are activated without the rupture reaching the terminus of the main fault.

From our maps, we estimate the passing probabilities of the different features as a function of their geometry, characterizing their potential as earthquake gates. Using these probability distributions, we analyze the joint probability of the observed breached gates and straight segments for each event and characterize the relationship of these probabilities to the observed surface rupture length.

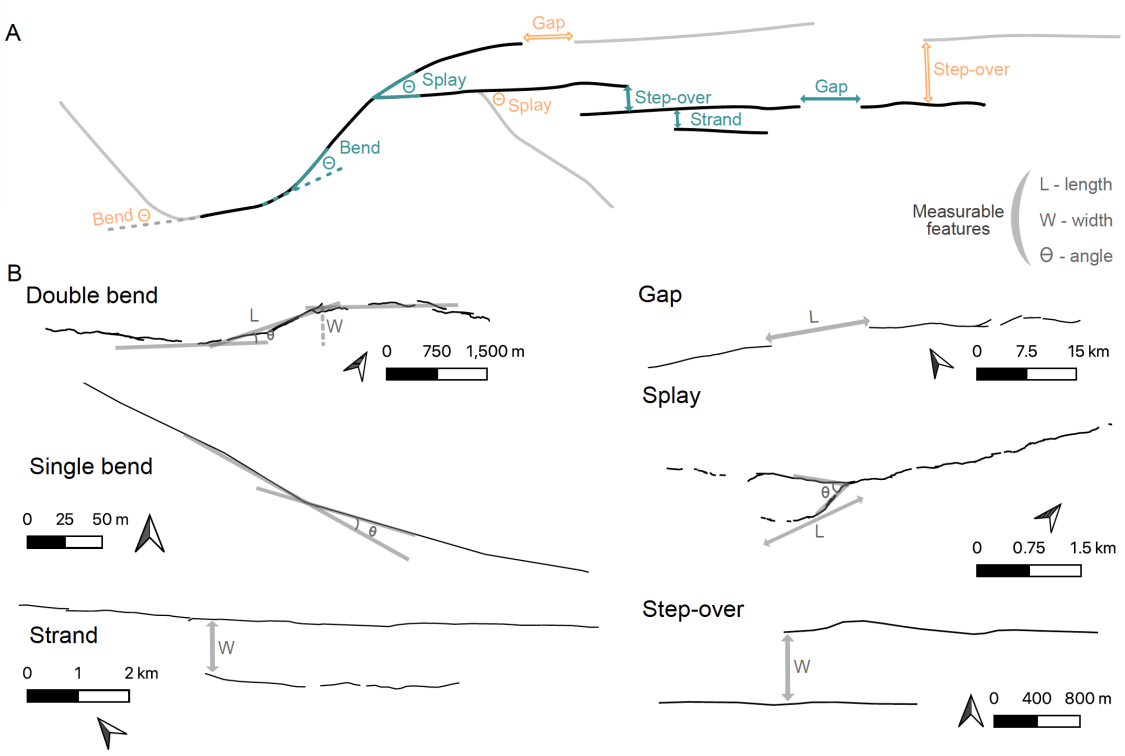

Figure 1. Geometrical complexity mapped in this study. (a) Simplified cartoon showing the features characterized. The black lines denote the surface rupture whereas the light gray lines represent the regional faults that did not rupture during the event. The widths, lengths, and angles measured are shown in teal for the breached features and in orange for the unbreached features. (b) Examples of breached features from the FDHI rupture map database (Sarmiento et al., 2021).

What geometrical complexities act as earthquake gates?

We classify each mapped feature as breached or unbreached, depending on whether the rupture propagated past the feature. To consider the size and geometry distribution of the earthquake gates we map, we estimate empirical cumulative distribution functions (ECDFs) for each population (Figure 2), separated into breached and unbreached groups, and restraining and releasing categories when possible. We infer that features with statistically distinct breached and unbreached populations are likely to act as earthquake gates, where passing probability is conditional in part on geometry. We use the two-sample Kolmogorov-Smirnoff (KS) test to assess whether different subset groups of an earthquake gate are statistically different. We use the p-value derived from the test, which is the probability of rejecting the null hypothesis that samples in the two subset groups were drawn from the same distribution. The convention here for statistical significance is $p<0.05$.

We mapped a total of 71 step-overs, where 26 are releasing and 45 are restraining. The widest breached step-over is ~1.8 km wide and restraining. The breached and unbreached step-over populations are distinct, though the restraining and releasing groups are statistically indistinguishable (p-values of ~0.5 and 0.7 for breached and unbreached populations respectively). We also map 7 strands, up to ~2 km away from the rupturing fault. We mapped a total of 130 gaps, where only 5 were unbreached. The largest breached gap is ~15 km long. Despite the low number of unbreached gaps mapped, the breached and unbreached ECDFs are statistically distinct (p-value of 0.01). Mapping an unbreached gap requires the rupturing fault and faults of parallel strike ahead of it to have been mapped in the regional map to a sufficient resolution to include gaps in the fault system. The low number of unbreached gaps we map may reflect the limited resolution of candidate, unactivated faults on available regional fault maps.

We map a total of 449 bends and analyze these separated into restraining versus releasing, and single versus double categories (Figure 2). The largest breached single bend is ~47° and the largest breached double bend is ~42°. The breached and unbreached single and double bends are statistically different ($p=3x10^{-17}$ and $p=0.005$), but the breached restraining and releasing populations are not (p-values of 0.1 and 0.7 for breached and unbreached respectively).

We map 47 splays. The angles of splays that were ruptured versus splays that were bypassed cannot be separated by the KS test ($p=0.7$). In most cases where a splay was activated,

the rupture propagated less than 3 km onto the splay fault. Modeling studies suggest rupture arrest at splays is related to the kinematics of the junction and the length of the fault branch (Poliakov et al., 2002; Kame et al., 2004). Though we do not classify our splays into transpressional or transtensional because the direction of rupture propagation is only known for some events, the fact that we only observe two complete rupture arrests at splays suggests that the presence of a splay plays a small role in the behavior of the rupture on the principal fault, despite the fact that most splay branches mapped were relatively short, which should hinder rupture propagation by allowing the two fault segments to interact as the rupture stops on the shorter one (Bhat et al., 2007). Overall, our results suggest that splays do not play an important role in rupture arrest at the mapping scale and that small splays may be surficial features without depth-persistence.

An important difference between characterizing step-overs from simplified rupture maps and the detailed rupture maps in the FDHI database is that the simplified rupture maps may not include linking structures. Breached step-overs wider than 2 km measured in previous work (e.g. Lettis et al., 2002) are hard-linked by faults in the more detailed rupture maps. We classify these hard-linked steps as breached double bends or splays, depending on what feature achieves the linkage. This is the case for the steps along the Landers earthquake which are hard linked by splay faults and were previously described as “complex step-overs” (e.g., Biasi and Wesnousky, 2016).

As part of their evolution, step-overs can become hard-linked by fault segments, evolving into double bends (Figure S1). We analyze our bend population by looking at two additional geometrical characteristics, a bend length (Lozos et al., 2011), and a proxy step-over width (Figure S1). When we parameterize bends by length or proxy step-over width, we find no clear differences between the breached and unbreached populations (Figure 2h, g). This suggests that step-overs that evolve into double bends become mechanically different features with higher passing probability for the same (proxy) width. An important implication of this observation is that the hard linkage we observe at the surface may persist at depth. This supports that earthquake gates of small dimensions can span the entire seismogenic zone and play a role in modulating rupture dynamics.

Rupture termination sometimes occurs on a straight portion of a fault, absent an observed earthquake gate, where the active fault continues for at least one kilometer past the rupture tip.

This is the case for ~20% of the rupture termini in this study, comparable to the 10% of Biasi and Wesnousky (2016), who used a five-kilometer threshold for rupture continuation.

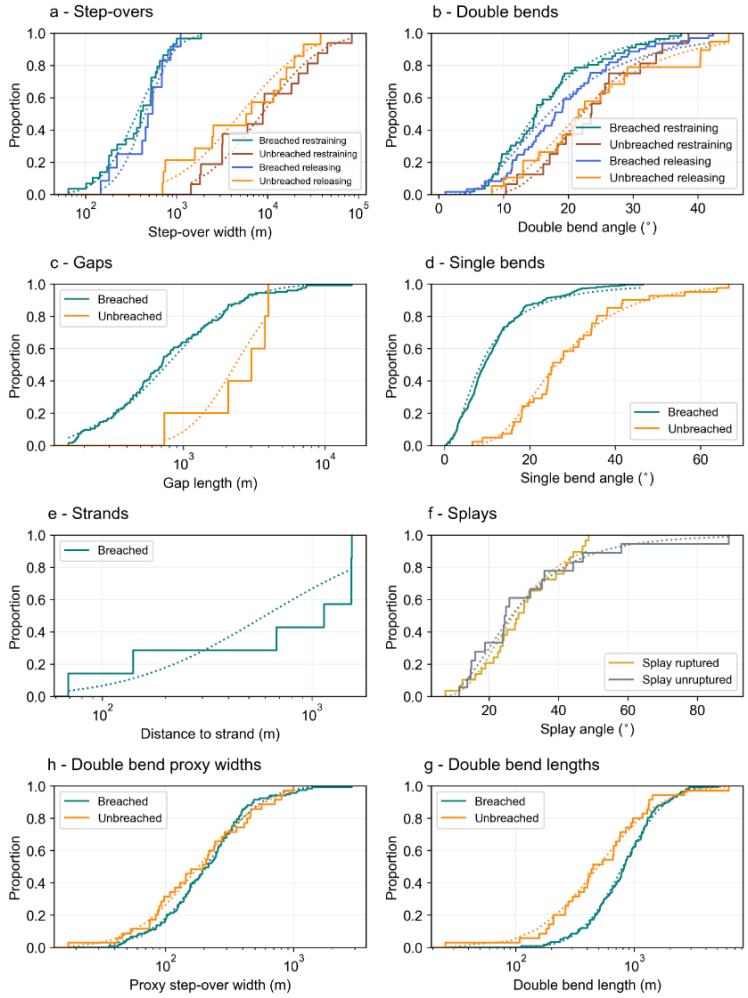

Figure 2. Empirical cumulative distribution function for the features mapped in this study (solid) and log-normal cumulative distribution fit for each ECDF (dotted). a: Restraining and releasing step-overs, parameterized based on width. b: Restraining and releasing double bends, parameterized based on angle. c: Gap length. d: Single bends, parametrized based on angle. e: Strands, parametrized based on their distance to the principal fault. f: Splays, separated into ruptured or unruptured and categorized by angle. g: Double bend proxy step-over width (Figures 1 and S1). h: Double bend length.

Passing probabilities of earthquake gates

Step-overs, gaps, and bends have statistically different breached and unbreached populations, acting as earthquake gates. We estimate passing probability as a function of geometry using a logistic model. This model describes the probability of a binary outcome (breached versus unbreached) as a continuous function of the geometrical properties of an earthquake gate, without requiring arbitrary binning of the data (see supplementary methods). We use unweighted logistic regressions despite the number of features in the breached and unbreached classes being different in the gaps and bends groups. We do this because, especially for the bends, the range of breached and unbreached bend angles largely overlaps, so that the relative frequency of breached and unbreached features is what distinguishes the two groups. Weighting the data inversely by frequency would obscure this effect.

Because restraining and releasing features are not statistically different, we combine these groups when estimating passing probabilities. Our logistic models (Figure 3) suggest that step-overs wider than ~1.2 km will be breached less than half of the time. Step-overs >5 km will be breached <1% of the time, consistent with the fact that they are not observationally documented without linking structures in the rupture maps. The logistic models predict that gaps longer than ~24.5 km will be breached less than half of the time. This distance is considerably larger than for step-overs, which we interpret as evidence that the absence of sufficient unbreached gap measurements precludes a robust estimate of passing probabilities for gaps, or that gaps are not earthquake gates. Double bends >38° and single bends >32° are predicted to be breached less than half of the time.

We assess the performance of our logistic regressions using an ROC score and confusion matrix (Pedregosa et al., 2011, supplementary methods, Figures 3 and S3). Both metrics support that step-over width is a strong predictor of rupture arrest. The logistic regressions struggle to predict unbreached bends well. This is because the populations of breached and unbreached bends largely span the same bend angles and are only separated by the changes in the breached and unbreached frequency of that angle, which makes it difficult to predict with a binary classifier. Therefore, at the mapping scale, only large bend angles (>40°) consistently halt earthquake ruptures.

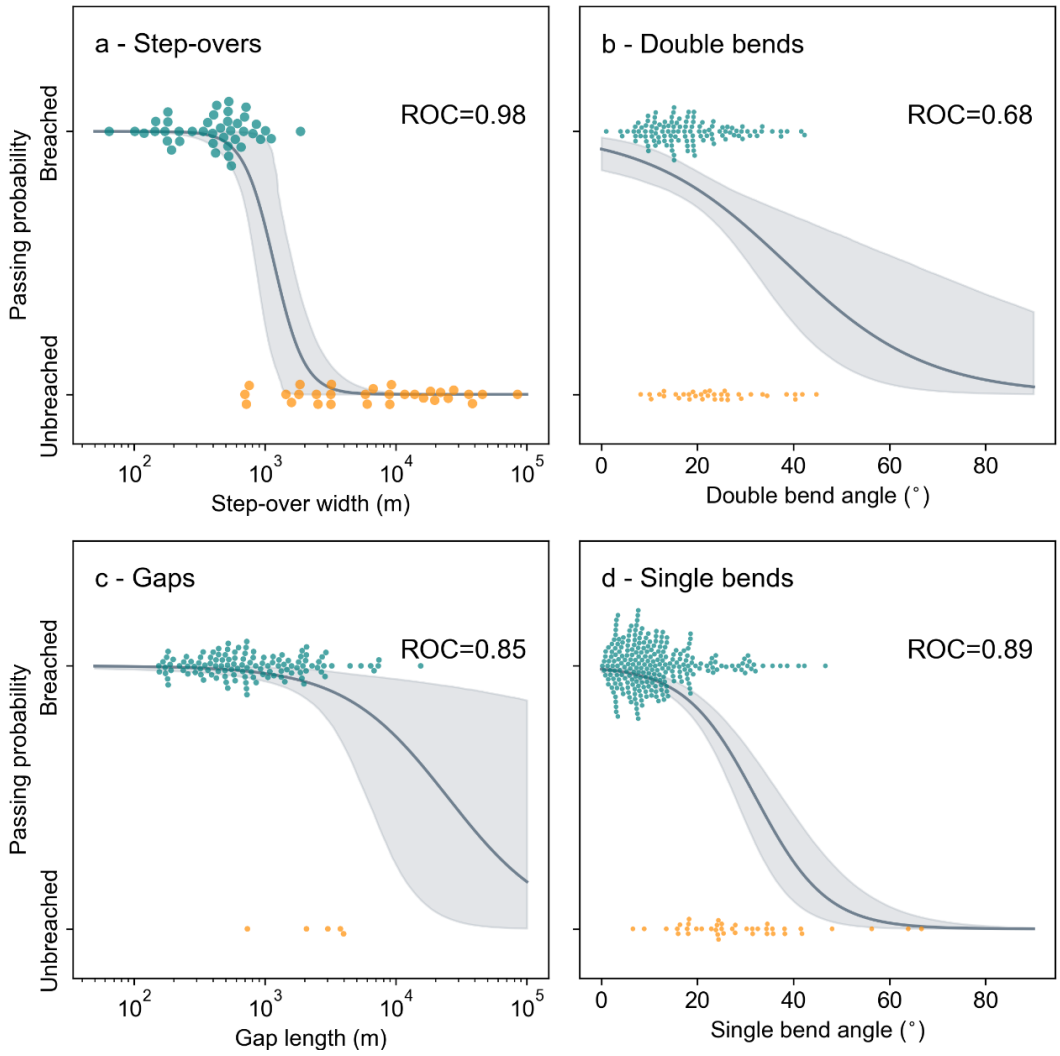

Figure 3. Logistic regressions (gray) showing the passing probabilities of geometrical features. The data are shown as beehive plots, which show all data points in each classification, breached in teal and unbreached in orange. Restraining and releasing features are combined (shown separately in Figure S2). a: Passing probability as a function of step-over width. b: Passing probability as a function of double bend angle. c: Passing probability versus gap length. d: Passing probability as a function of single bend angle. The gray shading shows the 95% confidence interval calculated by bootstrapping.

Biasi and Wesnousky (2016) predict step-overs wider than 3 km will be breached <50% of the time. Three kilometers exceeds our largest observed breached step-over, which is ~1.8 km wide. Biasi and Wesnousky (2017) also predict that bends sharper than 25° bend will be breached <50%. These finding are consistent with the estimate of Ozawa et al. (2023) using quasi-dynamic

rupture models (Figure S4). We predict much larger passing probabilities of ~70% for single and double bends of that size. The differences between our passing probabilities and those in previous work arise from the use of different rupture maps (simplified versus not) and mapping at a finer scale. Mechanically, breaching the larger bends we map may require a locally heterogeneous stress field, as the large angle change would make the bend segment very incompatible with a uniform stress field, even at low static friction values (Biasi and Wesnousky, 2017). A change in fault rake from strike-slip to dip-slip could also explain larger bend angles but we lack the data to test this option (see methods). Nevertheless, the fact that releasing and restraining features are statistically indistinguishable (Figure 2) is also consistent with a locally heterogeneous stress field, since homogeneous stress fields consistent yield distinctly different behavior for restraining and releasing features (e.g. Lozos et al., 2011).

Whether surficial fault geometry corresponds to that at depth is a challenge for using surface rupture maps to understand the physics of earthquake propagation. The different breached and unbreached populations and associated passing probabilities we obtain suggest a correlation between fault geometry at the surface and rupture propagation at depth. Together with the difference in rupture behavior through step-overs and double bends of the same dimensions, this suggests that the features we map at the surface, of 100-500 m length scales, extend downdip to the seismogenic zone.

Geometrical controls on surface rupture length

For each of the events examined, we model an event likelihood that reflects the pre-existing geometrical complexity in the hosting fault system as measured on the surface. We model event likelihood as the joint likelihood of continuing past the collective straight fault segments, $p(L)$, and breaching n gates each with passing probability p_i in an event: $P_{EQ} = P(L)\prod_{i=1}^{N} p_i$. We assume a constant chance of arrest at any point along without barriers and that the probabilities of stopping at different barriers are independent. Accordingly, the probability that segments reach a certain length in the absence of gates is the survival function of the exponential distribution, $p(L) = e^{-\lambda L}$ where L is the rupture length, and $\lambda = 1 \times 10^{-5}$ arrests/m is calculated by dividing the total number of arrests on straight segments by the total rupture length of all events. We derive passing probabilities for each feature as a function of its geometry from our logistic

models (Figure 3). We exclude gaps from the likelihood estimates given the small number of unbreached gaps sampled and the fact that they do not clearly behave as gates.

To investigate the relationship of rupture length to event likelihood, we compute likelihoods as cumulative probabilities along each mapped rupture (Figure 4a), following a similar approach to Biasi and Wesnousky (2021). As ruptures encounter earthquake gates, the cumulative log-likelihood of each event decreases. Because these ruptures are long, gates with high passing probabilities contribute largely to reducing the event likelihood, even if their role in rupture arrest is unlikely. The final likelihood of each event is well related to the rupture length exponentially (Figure 4a), where the average spacing between neighboring gates is ~2 km (Figure S5).

Earthquake scaling is typically considered in the context of the Gutenberg-Richter relationship, which predicts a power-law relationship between event frequency and rupture length (Figure 4a). Like in previous work on deriving probabilities from surface ruptures, the likelihood-length relationship does not match this prediction (Biasi and Wesnousky, 2021). With independent stopping probabilities at earthquake gates, as is inferred here, event likelihood will follow an exponential relationship, as opposed to a power law. To produce a power-law relationship would require that passing probabilities increase with rupture length, which is not supported by the observed distribution of earthquake gates (Figures 4a and S5). The Gutenberg-Richter relationship is defined for a population of earthquakes but may not fully describe the behavior of individual faults. Instead, each fault appears to have its own set of earthquake gates that contribute towards limiting rupture length. The possibility of non-Gutenberg-Richter behavior on a single fault is well-supported in the geological literature for surface-rupturing earthquakes (e.g. Schwartz and Coppersmith, 1984) but contrasts from the Gutenberg-Richter behavior associated with small earthquakes on single faults (Shelley et al., 2016). The distinction may have to do with the energetics of small versus seismogenic zone spanning events.

In this dataset, earthquakes often ended at barriers, where ~80% of the rupture termini occurred at earthquake gates, supporting that barriers play a fundamental role in rupture arrest (Aki, 1979, 1989; King and Nabelek, 1985; Klinger et al., 2006; Rockwell and Klinger, 2013). The distribution of breached barriers documented here also provide guidance on the appropriate model for rupture growth and propagation. An end-member model arising from linear elastic fracture mechanics is a crack with a uniform pre-stress in an infinite space, where the elastic

energy delivery rate would increase with rupture propagation length (e.g., Freund, 1998). In this model, stronger barriers would be required to stop rupture with greater propagation distance. We do not find a correlation between event size and barrier size, or barrier size along the rupture (Figures S6, S7 and S8). Therefore, this end-member is likely not appropriate and some heterogeneity in the stress field is required. An alternative crack-model with pre-stressed asperities results in a variable energy delivery rate (Lay and Kanamori, 1981; Li et al., 2023). Under this model, the available elastic energy is supplied by the asperities and decreases as the rupture propagates into regions with smaller pre-stress (Figure 4b). Seismological evidence supports that large surface rupturing events may be fueled by several asperities along the rupture (e.g. Li et al., 2023). This model predicts that larger gates would be breached in proximity to asperities, where the energy delivery rate is largest. We find no relationship between the geometry of breached gates and the distance to the event epicenter or the amplitude of the displacement, proxies for the locations of asperities (Figures S9 and S10), though the displacement data is limited for older events and certain regions. Pulses offer a third alternative. Ruptures tend to propagate as pulses once the seismogenic zone has been saturated (e.g. Heaton, 1990; Melgar and Hayes, 2017; Weng and Ampuero, 2019), which would result in a constant energy release rate under a homogeneous stress field. This model is consistent with the lack of correlation between breached gate size and location along the rupture, but incomplete, as some of our observations require a heterogeneous pre-stress distribution (e.g., large breached bend angles and indistinguishable releasing and restraining features). A propagating pulse encountering a collection of asperities of variable size that provide a variable energy delivery rate can explain both the observations requiring a heterogeneous pre-stress on the fault, and the absence of strong spatial relationships for the distribution of breached earthquake gates on the fault. Dynamic rupture models incorporating a distribution of earthquake gates similar to that described may provide a future test of this hybrid model.

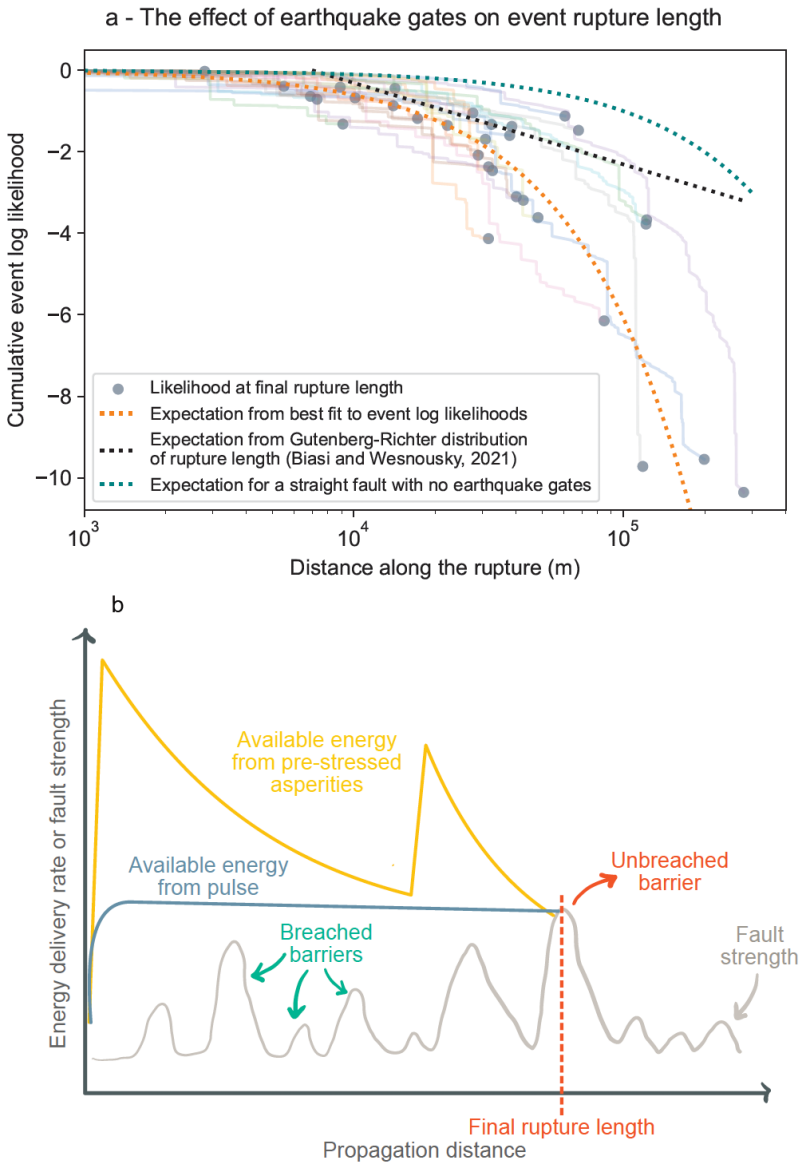

Figure 4. a: Cumulative event likelihood versus distance along the surface rupture. Each colored line represents one event. The scattered dots indicate the event likelihood at its final rupture length. The rupture lengths are based on the FDHI event coordinate system (ECS) reference lines (Sarmiento et al., 2021). The orange line represents the best fit to the final event likelihoods. The black line represents the predicted decrease in event likelihood with rupture length using the Gutenberg-Ritcher relationship for magnitude scaling. All likelihoods estimated using base *e*. b: Schematic cartoon of how an earthquake gate will bring rupture to arrest, conditional on the available elastic energy being lower than the strength of the barrier. Schematic elastic energy for a crack with two pre-stressed asperities and a pulse in a homogeneous stress field shown.

When an earthquake terminates at a barrier, elevated residual stresses, if not relaxed, can promote rupture propagation past the barrier in a future event. This behavior is observed in multi-cycle rupture models (e.g., Duan and Oglesby, 2006; Molina-Ormazabal et al., 2023), laboratory experiments (Cebry et al., 2023), and inferred from the occurrence of aftershocks at barriers where ruptures terminate (Aki, 1979). Earthquake gates may therefore act as a barrier during an event, and as an asperity in a future one. The data in this study only permit assessing the behavior of individual gates over one earthquake cycle, but considering the data together offers insights into the frequency over which earthquake gates may act as an energy source, overlapping with locations of high slip on the fault, or energy sinks, overlapping with locations of low slip. We find that most of the large earthquake gates correspond with locations of low slip (Figure S10), consistent with ubiquitous barrier behavior, though small gates span a wide range of slip values. The very rare overlap of high slip values and unbreached earthquake gates suggests that, while earthquake gates may also act as asperities, this relationship is not frequent enough or the effect sufficiently large to stand out in our surface-rupture dataset. This is consistent with recent experimental work by Cebry et al. (2023), which showed that a high normal stress bump (a bend) behaved most frequently as a barrier but occasionally as an energy source, or asperity.

Conclusions

We map step-overs, bends, gaps, splays, and strands along the surface rupture maps of 31 strike-slip earthquakes at 1:50,000 scale, labeling these features as breached and unbreached. We use these measurements to fit a logistic model to each feature that estimates passing probabilities as a function of geometry. Step-over width as measured at the surface is an excellent predictor of arrest. Bend angle is a worse predictor, although the ratio of unbreached to breached bends increases consistently with increasing bend angle. The fact that gates are preferred stopping points provides evidence that the surficial features can persist to depth. A more direct test of this idea is provided by the different behavior of step-overs and double bends of the same (proxy) width, which suggests that step-overs persist as discrete unlinked fault strands at depth. Our results call for models with geometrically complex faults consistent with our mapping scale to explore what dynamic rupture conditions may match our passing probabilities.

We use earthquake gate passing probabilities in each event to build an empirical model for

the growth and arrest of large earthquakes given the complexity of the hosting fault system. The cumulative event likelihood tabulated along rupture strike supports a barrier model as a factor in controlling earthquake size, where relatively straight fault segments are bounded by geometrical barriers that must be breached for the rupture to continue growing.

Acknowledgments

We are grateful for comments from Julian Lozos and Glenn Biasi. We thank Coby Abrahams, Will Steindhart, Jean-Philippe Avouac, and Alexis Saez for suggestions and So Ozawa for sharing his data. S.W., V.H., and A.M.R.P. benefitted from mentoring from Gaby Noriega. A.M.R.P was supported by NASA FINESST award 80NSSC21K1634.

Open Research

The rupture maps are available from the FDHI database (Sarmiento et al., 2021), accessed May 2022. Data and code can be accessed at Data and code. All materials will be transferred to a Zenodo repository for permanent storage following acceptance.

References

1. Aki, K. (1979). Characterization of barriers on an earthquake fault. Journal of Geophysical Research: Solid Earth, 84(B11), 6140-6148.
2. Aki, K. (1989). Geometric features of a fault zone related to the nucleation and termination of an earthquake rupture. In Proceedings of Conference XLV. Fault Segmentation Controls of Rupture Initiation and Termination (pp. 1-9).
3. Bachmanov, D.M., Trifonov, V.G., Kozhurin, A.I. and Zelenin E.A.: AFEAD v.2021 Active Faults of Eurasia Database, https://doi.org/10.13140/RG.2.2.10333.74726, 2021.
4. Biasi, G. P., & Wesnousky, S. G. (2016). Steps and gaps in ground ruptures: Empirical bounds on rupture propagation. Bulletin of the Seismological Society of America, 106(3), 1110-1124.
5. Biasi, G. P., & Wesnousky, S. G. (2017). Bends and ends of surface ruptures. Bulletin of the Seismological Society of America, 107(6), 2543-2560.
6. Biasi, G. P., & Wesnousky, S. G. (2021). Rupture passing probabilities at fault bends and steps, with application to rupture length probabilities for earthquake early warning. Bulletin

of the Seismological Society of America, 111(4), 2235-2247.

7. Cebry, S. B., Sorhaindo, K., & McLaskey, G. C. (2023). Laboratory earthquake rupture interactions with a high normal stress bump. *Journal of Geophysical Research: Solid Earth*, *128*(11), e2023JB027297.
8. Crone, A. J., Personius, S. F., Craw, P. A., Haeussler, P. J., & Staft, L. A. (2004). The Susitna Glacier thrust fault: Characteristics of surface ruptures on the fault that initiated the 2002 Denali fault earthquake. Bulletin of the Seismological Society of America, 94(6B), S5-S22.
9. Davy, P. (1993). On the frequency-length distribution of the San Andreas fault system. *Journal of Geophysical Research: Solid Earth*, *98*(B7), 12141-12151.
10. Duan, B., & Oglesby, D. D. (2006). Heterogeneous fault stresses from previous earthquakes and the effect on dynamics of parallel strike-slip faults. *Journal of Geophysical Research: Solid Earth*, *111*(B5).
11. Field, E. H., Biasi, G. P., Bird, P., Dawson, T. E., Felzer, K. R., Jackson, D. D., ... & Zeng, Y. (2015). Long-term time-dependent probabilities for the third Uniform California Earthquake Rupture Forecast (UCERF3). *Bulletin of the Seismological Society of America*, *105*(2A), 511-543.
12. Field, E. H., Jordan, T. H., Page, M. T., Milner, K. R., Shaw, B. E., Dawson, T. E., ... & Thatcher, W. R. (2017). A synoptic view of the third Uniform California Earthquake Rupture Forecast (UCERF3). *Seismological Research Letters*, *88*(5), 1259-1267.
13. Hamling, I. J., Hreinsdóttir, S., Clark, K., Elliott, J., Liang, C., Fielding, E., ... & Stirling, M. (2017). Complex multifault rupture during the 2016 M w 7.8 Kaikōura earthquake, New Zealand. Science, 356(6334), eaam7194.
14. Heaton, T. H. (1990). Evidence for and implications of self-healing pulses of slip in earthquake rupture. *Physics of the Earth and Planetary Interiors*, *64*(1), 1-20.

15. King, G., & Nábělek, J. (1985). Role of fault bends in the initiation and termination of earthquake rupture. Science, 228(4702), 984-987.
16. Klinger, Y., Michel, R., & King, G. C. (2006). Evidence for an earthquake barrier model from Mw~7.8 Kokoxili (Tibet) earthquake slip-distribution. Earth and Planetary Science Letters, 242(3-4), 354-364.

17. Klinger, Y. (2010). Relation between continental strike-slip earthquake segmentation and thickness of the crust. Journal of Geophysical Research: Solid Earth, 115(B7).
18. Langridge, R. M., Ries, W. F., Litchfield, N. J., Villamor, P., Van Dissen, R. J., Barrell, D. J. A., ... & Stirling, M. W. (2016). The New Zealand active faults database. New Zealand Journal of Geology and Geophysics, 59(1), 86-96.
19. Lay, T., & Kanamori, H. (1981). An asperity model of large earthquake sequences. *Earthquake prediction: An international review*, *4*, 579-592.
20. Lettis, W., Bachhuber, J., Witter, R., Brankman, C., Randolph, C. E., Barka, A., ... & Kaya, A. (2002). Influence of releasing step-overs on surface fault rupture and fault segmentation: Examples from the 17 August 1999 Izmit earthquake on the North Anatolian fault, Turkey. *Bulletin of the Seismological Society of America*, *92*(1), 19-42.
21. Lienkaemper, J. J., Pezzopane, S. K., Clark, M. M., & Rymer, M. J. (1987). Fault fractures formed in association with the 1986 Chalfant Valley, California, earthquake sequence: preliminary report. Bulletin of the Seismological Society of America, 77(1), 297-305.
22. Li, J., Kim, T., Lapusta, N., Biondi, E., & Zhan, Z. (2023). The break of earthquake asperities imaged by distributed acoustic sensing. *Nature*, *620*(7975), 800-806.
23. Lozos, J. C., Oglesby, D. D., Duan, B., & Wesnousky, S. G. (2011). The effects of double fault bends on rupture propagation: A geometrical parameter study. Bulletin of the Seismological Society of America, 101(1), 385-398.
24. Manighetti, I., Campillo, M., Bouley, S., & Cotton, F. (2007). Earthquake scaling, fault segmentation, and structural maturity. Earth and Planetary Science Letters, 253(3-4), 429-438.
25. Melgar, D., & Hayes, G. P. (2017). Systematic observations of the slip pulse properties of large earthquake ruptures. *Geophysical Research Letters*, *44*(19), 9691-9698.
26. Milner, K. R., Shaw, B. E., & Field, E. H. (2022). Enumerating plausible multifault ruptures in complex fault systems with physical constraints. *Bulletin of the Seismological Society of America*, *112*(4), 1806-1824.
27. Molina-Ormazabal, D., Ampuero, J. P., & Tassara, A. (2023). Diverse slip behaviour of velocity-weakening fault barriers. *Nature Geoscience*, *16*(12), 1200-1207.
28. Nurminen, F., Baize, S., Boncio, P., Blumetti, A. M., Cinti, F. R., Civico, R., & Guerrieri, L. (2022). SURE 2.0–New release of the worldwide database of surface ruptures for fault

displacement hazard analyses. *Scientific Data*, *9*(1), 729.

29. Ozawa, S., Ando, R., & Dunham, E. M. (2023). Quantifying the probability of rupture arrest at restraining and releasing bends using earthquake sequence simulations. *Earth and Planetary Science Letters*, *617*, 118276.
30. Pedregosa, F., Varoquaux, G., Gramfort, A., Michel, V., Thirion, B., Grisel, O., ... \& Duchesnay, E. (2011). Scikit-learn: Machine learning in Python. the Journal of machine Learning research, 12, 2825-2830.
31. Perrin, C., Manighetti, I., Ampuero, J. P., Cappa, F., & Gaudemer, Y. (2016). Location of largest earthquake slip and fast rupture controlled by along-strike change in fault structural maturity due to fault growth. Journal of Geophysical Research: Solid Earth, 121(5), 3666-3685.
32. Rockwell, T. K., & Klinger, Y. (2013). Surface rupture and slip distribution of the 1940 Imperial Valley earthquake, Imperial fault, southern California: Implications for rupture segmentation and dynamics. Bulletin of the Seismological Society of America, 103(2A), 629-640.
33. Sarmiento, A., Madugo, D., Bozorgnia, Y., Shen, A., Mazzoni, S., Lavrentiadis, G., Dawson, T., Madugo, C., Kottke, A., Thompson, S., Baize, S., Milliner, C., Nurminen, F., Boncio, P., and Visini, F. (2021). Fault Displacement Hazard Initiative Database, UCL B. John Garrick Institute for the Risk Sciences, Report GIRS-2021-08, doi: 10.34948/N36P48.
34. Schwartz, D. P., & Coppersmith, K. J. (1984). Fault behavior and characteristic earthquakes: Examples from the Wasatch and San Andreas fault zones. *Journal of Geophysical Research: Solid Earth*, *89*(B7), 5681-5698.
35. Shelly, D. R., Ellsworth, W. L., & Hill, D. P. (2016). Fluid-faulting evolution in high definition: Connecting fault structure and frequency-magnitude variations during the 2014 Long Valley Caldera, California, earthquake swarm. *Journal of Geophysical Research: Solid Earth*, *121*(3), 1776-1795.
36. Styron, R., & Pagani, M. (2020). The GEM global active faults database. Earthquake Spectra, 36(1), 160-180.
37. U.S. Geological Survey, 2020, Quaternary Fault and Fold Database for the Nation, accessed [August, 10, 2022], at https://doi.org/10.5066/P9BCVRCK

462 38. Wells, D. L., & Coppersmith, K. J. (1993). Likelihood of surface rupture as a function of
463 magnitude. Seismological Research Letters, 64(1), 54.
464 39. Wechsler, N., Ben-Zion, Y., & Christofferson, S. (2010). Evolving geometrical
465 heterogeneities of fault trace data. *Geophysical Journal International*, *182*(2), 551-567.
466 40. Weng, H., & Ampuero, J. P. (2019). The dynamics of elongated earthquake
467 ruptures. *Journal of Geophysical Research: Solid Earth*, *124*(8), 8584-8610.
468 41. Wesnousky, S. G. (1988). Seismological and structural evolution of strike-slip faults.
469 Nature, 335(6188), 340-343.
470 42. Wesnousky, S. G. (2006). Predicting the endpoints of earthquake ruptures. Nature,
471 444(7117), 358-360.
472 43. Wesnousky, S. G. (2008). Displacement and geometrical characteristics of earthquake
473 surface ruptures: Issues and implications for seismic-hazard analysis and the process of
474 earthquake rupture. Bulletin of the Seismological Society of America, 98(4), 1609-1632.

Geophysical Research Letters

Supporting Information for

The influence of earthquake gates on surface rupture length

A.M. Rodriguez Padilla [1,2*], M.E. Oskin[1], E.E. Brodsky[3], K. Dascher-Cousineau[4], V. Herrera[5], S. White[6,7]

[1] Department of Earth and Planetary Sciences, University of California, Davis

[2] Now at Division of Geological and Planetary Sciences, California Institute of Technology

[3] Department of Earth and Planetary Sciences, University of California, Santa Cruz

[4] Department of Earth and Planetary Sciences, University of California, Berkeley

[5] Department of Earth and Environmental Sciences, San Diego State University

[6] Geology Department, Pasadena City College

[7]Now at Department of Earth, Planetary, and Space Sciences, University of California, Los Angeles

*Corresponding author: Alba M. Rodriguez Padilla (alba@caltech.edu, amrodriguezpadilla@gmail.com)

Contents of this file

Introduction

This file contains the mapping method followed, supplementary figures S1 to S11, table S12, and the maps of each event and its corresponding earthquake gate. The maps are generated in 30 x 30 in files at 300 dpi so that they can be easily zoomed into and examined.

Supplementary Methods

Earthquake Gate Mapping

We choose to focus on strike-slip events because vertically dipping faults tend to remain constant in dip with depth so that surface geometry, besides fine-scale heterogeneity, can be used as a proxy for the geometry at depth. We rely on the surface rupture maps compiled in the Fault Displacement Hazard Initiative (FDHI) database (Sarmiento et al., 2021). At the time of access for this manuscript (May, 2022), the database encompassed sixty-six, globally distributed, surface rupturing earthquakes (M_w 5-8), of which thirty-one are strike-slip. The database includes surface rupture maps for each event, were ruptures are classified as primary or distributed, displacement measurements, and additional information, such as lithology or slope. Surface ruptures are mapped to 1-meter precision in the database, though individual maps differ in the level of detail captured in the surface rupture. This variability is in part related to the different degrees of complexity in the hosting fault system, and in part a result of differences in mapping methods and extent across ruptures.

We map earthquake gates from the surface ruptures in the FDHI database at a 1:50,000 scale, which roughly corresponds to mapping features with lengths exceeding 100-500 meters. At this scale, we expect the level of detail across ruptures to be roughly comparable. The surface rupture maps in the FDHI database include ruptures classified as principal and distributed. To ensure that we only include primary faults, which are the seismogenic structures in the events in our analysis, we consider the ruptures characterized as principal in the database. This also allows for comparison across events with different spatial coverage of the off-fault deformation field.

Prior work has either relied on simplified rupture maps (e.g., Wesnousky, 2006) or simplified ruptures to segments long enough (~7 km) to make results commensurable with UCERF3 model discretization and comparable to standard fault maps (Biasi and Wesnousky, 2017, 2021). We map earthquake gates directly from the surface rupture maps, without simplifying the rupture traces. An important consequence of our scale of choice (1:50,000) is that larger features (for example, the large, regional-scale releasing bend in the Balochistan earthquake which spans 6 km) are mapped into its smaller constituents that occur at the mapping scale (i.e. several shorter bends that make up the regional one). Our scale of choice results in the mapping of smaller step-overs that were previously not classified in prior work due to their small size but does not

influence the maximum breached step-over width that can be measured as long as the step is not hard-linked, in which case it would be mapped as a bend or a splay.

We characterize gates as restraining or releasing when possible, depending on the volumetric deformation fostered by the type of slip and the geometry of the fault segments. To do this, we assume all fault segments involved in the rupture have strike-slip kinematics consistent with the focal mechanism for the event. At large scales, this is a reasonable approximation for all the strike-slip ruptures in the FDHI database except for the Denali earthquake, from which we remove the portion of the rupture that occurred on the Susitna Glacier Thrust, where the earthquake initiated (e.g., Crone et al., 2004). However, at finer scales, including our mapping scale, transitions from strike-slip to more oblique or vertical slip can lead to larger bend angles. We do not account for this limitation due to the absence of information to do so consistently for all events, following the rationale of Biasi and Wesnousky (2017).

A portion of the Kobe earthquake ruptured offshore and is not available in our map, with the section being onshore also being only a partial rupture to the surface, resulting in comparatively short surface rupture for the event magnitude. Incomplete rupture to the surface is also a limitation that applies to the smaller magnitude events considered here, such as the Chalfant Valley earthquake.

We characterize five different types of earthquake gates in this study: step-overs, gaps, bends, splays, and strands (Figure 1). We distinguish between breached features where the rupture transferred through and continued for at least 1 kilometer, and unbreached features, where the rupture halted immediately or within 1 km past the gate. For the case of splays, we classify cases where the rupture transferred onto a splay (regardless of whether it also continued on the main fault), as ruptured and instances where an available intersecting splay fault was foregone as unruptured. Note the use of different terminology from breached and unbreached to indicate that at least one fault strand was always active past the splay (Figure 1).

For each of the gates of interest, we measure the relevant geometrical attribute. For bends and splays, this is the bend angle, which is the difference between the fault strike as it enters the feature and the fault strike as it exits the feature. In the case of multi-stranded bends, we map the bend strand with the smallest angle. We distinguish between single bends, where the fault strike changes once, and double bends, where the fault strike changes for a segment and then returns to the original strike (see examples in Figure 1). Because natural double bends have angles that are

not perfectly identical on each side of the bend limb, we take the average of the two angles. In most cases, the angle difference between the two angles is well below 10 degrees. Step-overs occur where a fault ends and the rupture is forced to jump onto a neighboring segment or come to arrest. We also map locations where the rupture activates parallel to subparallel neighboring fault strands without reaching the terminus of the principal fault. By definition, strands may only exist as breached features, as there was no fault terminus that forced a jump. For step-overs and strands, we measure the distance between parallel or subparallel fault segments at their minimum, orthogonal to the fault segments when possible. For gaps, we measure the length of the gap between the active rupture and another fault, or between parts of the active rupture if breached, in the fault-parallel direction. Note that we do not have the ability to distinguish gaps that represent pauses on the rupture on the same fault versus gaps that represent the spacing between two sequential faults of parallel strike.

We rely on different active fault databases to characterize unbreached features, where we measure the angle or distance between the ruptured fault and unruptured active faults in the database. The reference databases we use are listed in Supplementary Table S11. For the United States, the resolution of the regional faults associated with the events in this study in the Qfaults database is comparable to the resolution of the primary rupturing faults in the FDHI database. For the Darfield event in New Zealand, we use the NZAFD database, mapped at 1:250,000 (Langridge et al., 2016). The Active Faults of Eurasia Database (AFEAD) database for Eurasia, which we use for events in Turkey and Asia, is mapped at 1:500,000 scale (Bachmanov et al., 2021). Last, the GEM database, which we use only for the San Miguel and Pisayambo earthquakes in Mexico and Ecuador respectively, is mapped at 1:1,000,000 scale (Styron and Pagani, 2020). In the interest of classifying unbreached features as restraining or releasing, when the inactive fault kinematics are unknown, we assume these are the same as the rupturing faults'. When two unbreached step-overs may be measured at a fault's terminus, we map both, following the choice of previous workers (e.g., Wesnousky, 2006). Note that some events (e.g., Galway Lake and Ridgecrest foreshock) have unbreached step-overs at both of their termini with the same fault (e.g., the faults in the Landers event and the Garlock fault respectively), in which case both unbreached step-overs are mapped. When a gap and a step-over of the same size exist, and one gets breached but the other one does not, we map both the breached and unbreached features. The same occurs where there is a bend but the rupture instead skips the bend and jumps ahead to a more straight portion of the

fault. This only occurs in the case of very similarly sized earthquake gates available at the same location, otherwise, we only map the smallest gate present. We provide our mapped earthquake gates as shapefiles (see data availability section) and shown over the rupture maps and regional fault maps in this supplementary section.

Passing Probability and Event Likelihood Estimates

To determine whether the forms of geometrical complexity we map (Figure 1) act as barriers to rupture propagation, we analyze the distribution of breached and unbreached gates in terms of the geometrical attribute measured (angle or length). We look at the cumulative distribution functions of breached and unbreached gates and use a Kolmogorov-Smirnoff (KS) test to determine whether the breached and unbreached populations are statistically different.

For those features where the breached and unbreached populations are statistically different (Figure 2), we compute passing probabilities as a function of the geometrical characteristics of the gate. To do so, we use a logistic function, which describes the probability of a binary outcome (breached or unbreached) as a continuous function of the geometry of an earthquake gate. To fit logistic regressions through our data, we use the Python package scikit learn (Pedregosa et al., 2011). An advantage of using logistic regressions over past methods is that estimating probabilities does not rely on arbitrary binning of the data. We evaluate the performance of our logistic models for each type of earthquake gate using Receiver Operating Characteristic (ROC) scores and confusion matrices, which is standard procedure for these models (Pedregosa et al., 2011). ROC scores can range from 0.5 to 1, with increasing values indicating that more data points have been correctly predicted by the logistic regression.

Supplementary Figures

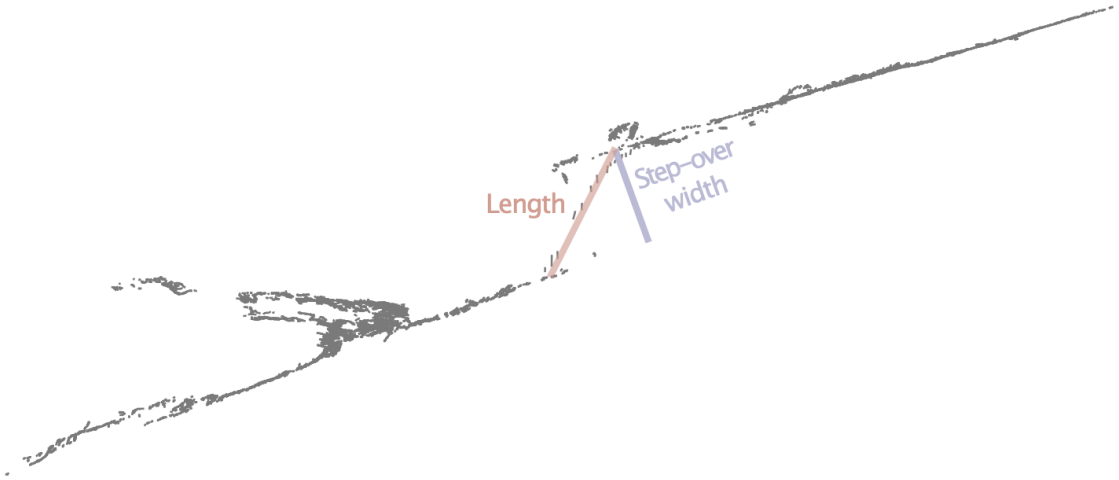

Figure S1. Releasing double bend from the 2014 Yutian earthquake. The rupture map is shown in gray. The pink and purple lines show the bend length as defined by Lozos et al. (2011) and the proxy step-over width respectively. The proxy step-over width is ~2.5 km wide.

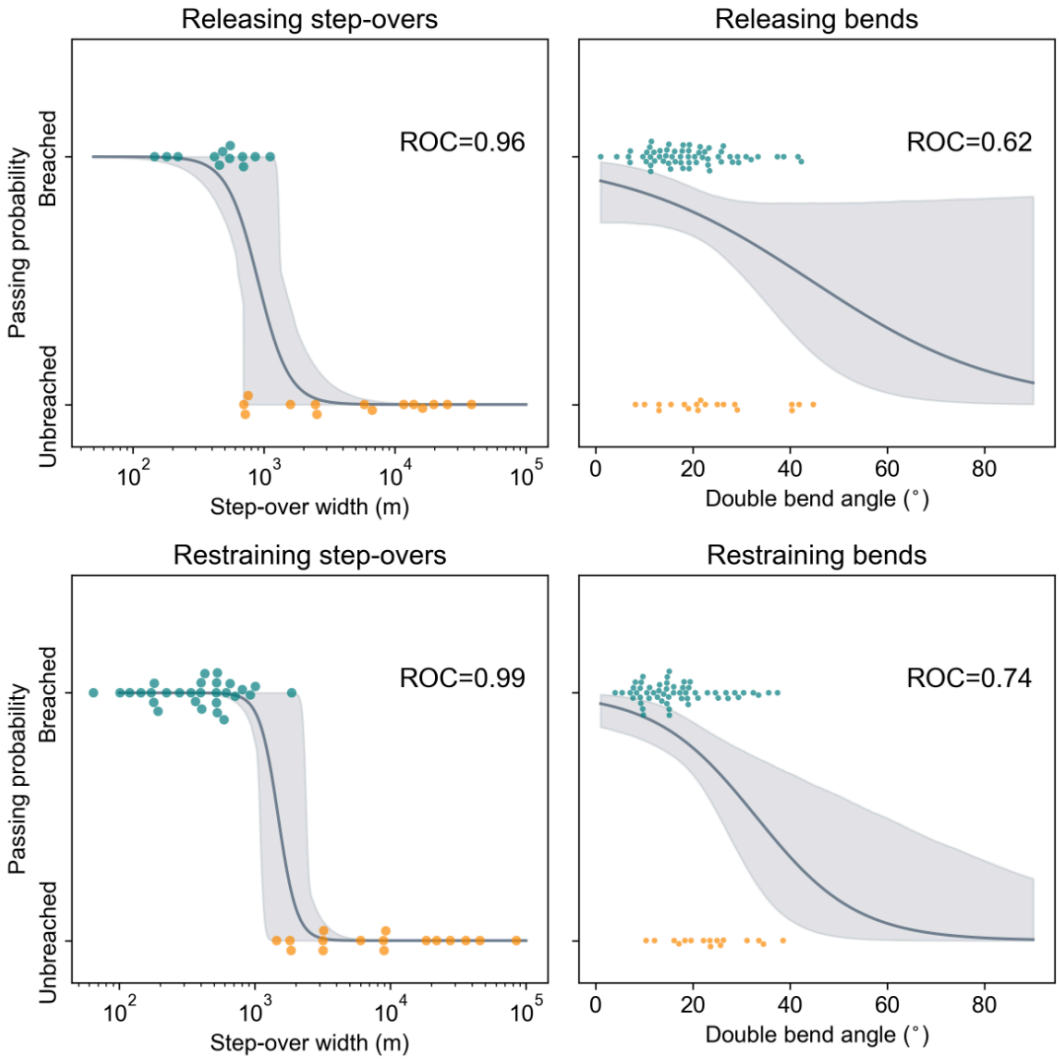

Figure S2. Logistic regressions (gray) showing the passing probabilities of restraining and releasing step-overs and double bends. The data are shown as beehive plots, which show all data points in each classification, breached in teal and unbreached in orange. The ROC score for each logistic regression is shown on the top right of each panel. Top and bottom left: Passing probability as a function of step-over width. Top and bottom right: Passing probability as a function of double bend angle. The gray shading shows the 95% confidence intervals of the regressions calculated by bootstrapping.

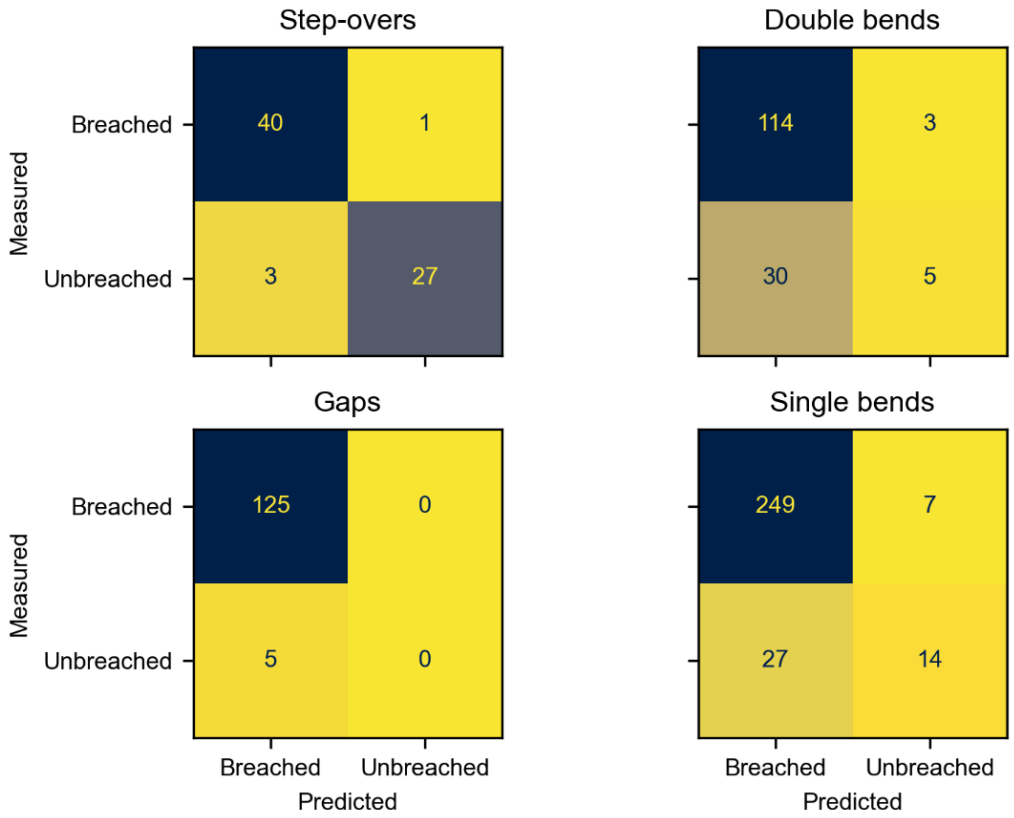

Figure S3. Confusion matrices for the logistic models for step-overs, single and double bends, and gaps in Figure 3. Darker colors in the matching diagonals indicate better diagnosis of the breached and unbreached features by the logistic fits.

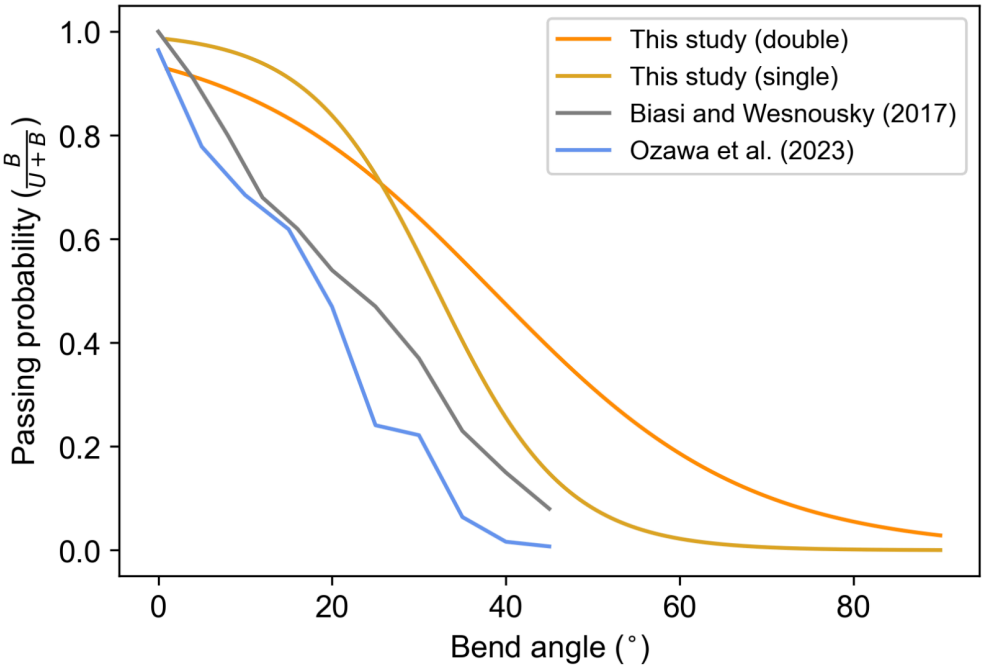

Figure S4. Comparison of the passing probabilities for different bend angles estimated in Biasi and Wesnousky (2017), Ozawa et al. (2023), and this study. Passing probability estimated as the number of breached bends per bin over the total number of bends in that bin in previous studies and with logistic regressions here. Note that the Biasi and Wesnousky (2017) passing probabilities include both single and double bends without discriminating between them, and the Ozawa et al. (2023) passing probabilities only include double bends.

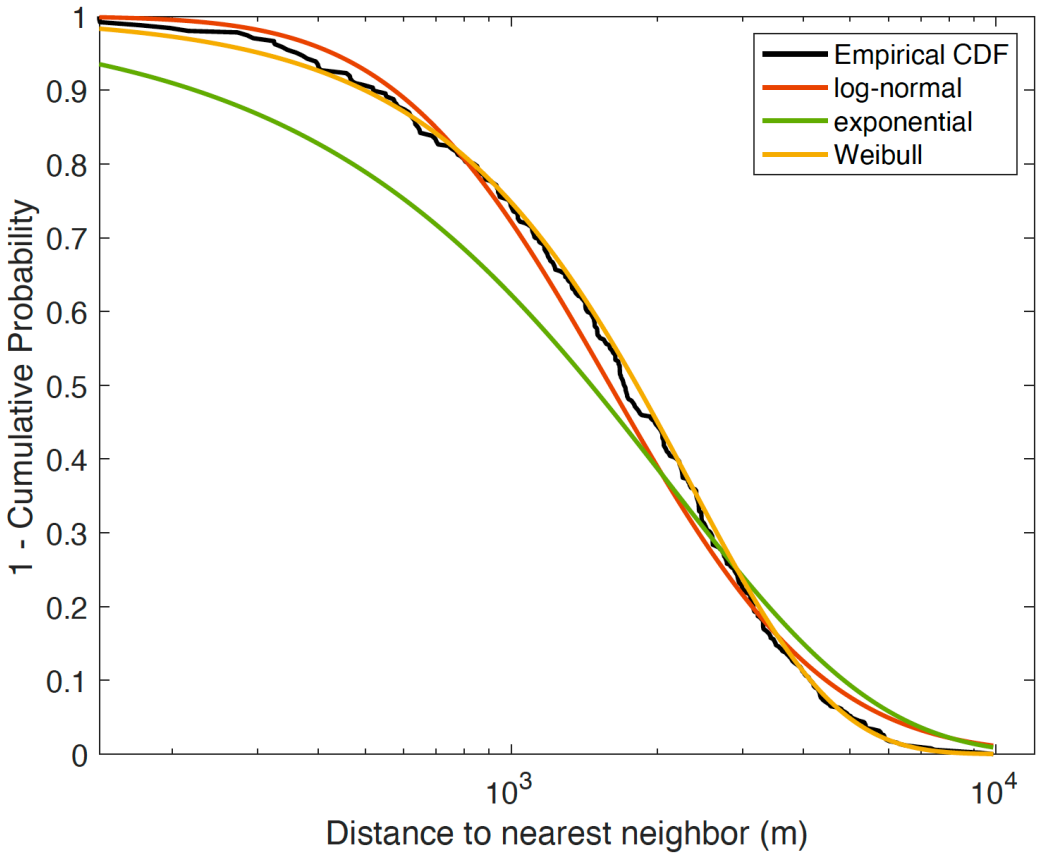

Figure S5. Empirical complementary cumulative distribution function of the distances to nearest neighbor for all breached earthquake gates. Complementary cumulative distribution functions for a log-normal, an exponential, and a Weibull fit are shown in orange, green, and yellow, respectively.

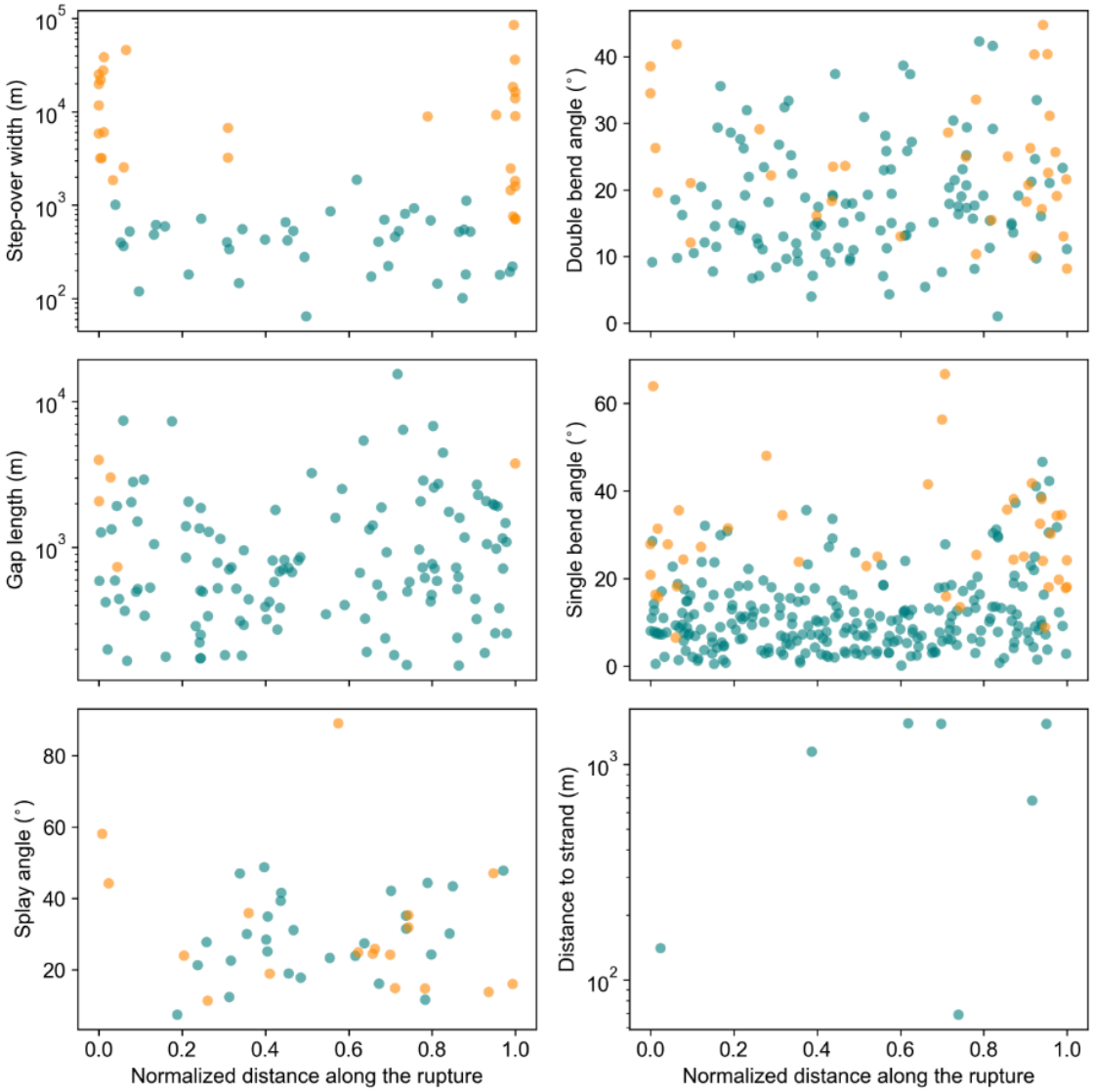

Figure S6. Distribution of breached (teal) and unbreached (orange) earthquake gates along the normalized surface rupture lengths of the 31 strike-slip events. The rupture lengths are based on the FDHI database event coordinate systems (ECS) reference lines (Sarmiento et al., 2021). There are some unbreached gates not at the edge of the ruptures. This is because, at some locations, there were two or more earthquake gates available, so that the gate the rupture continues past is mapped as breached and the remaining ones get mapped as unbreached (see methods for details).

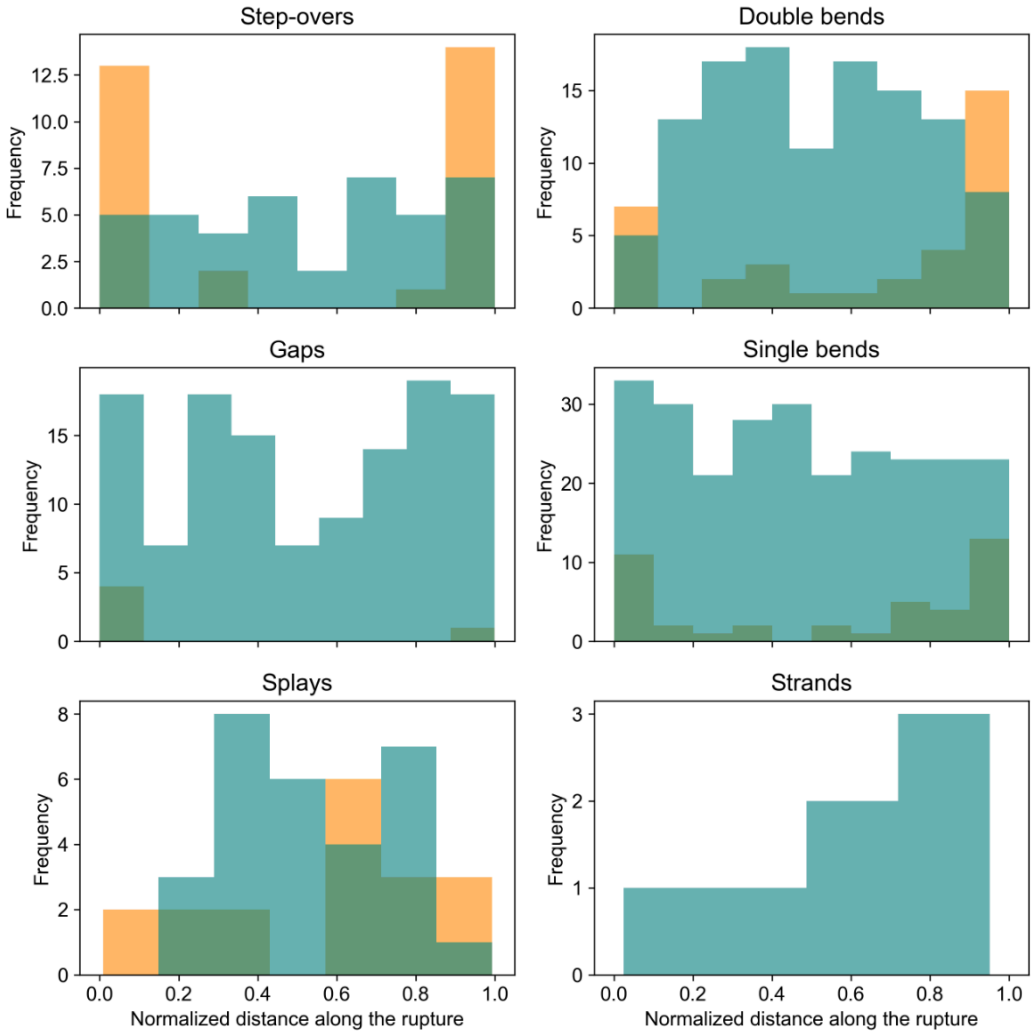

Figure S7. Frequency of earthquake gates, breached and unbreached in teal and orange respectively, along the normalized surface rupture length for each earthquake gate type. Transparency is used to allow for visualization of the unbreached boxes (orange). Because we do not consider rupture propagation direction, as it is unknown for many of the events, the orientation of the x axis of this plot does not carry meaning.

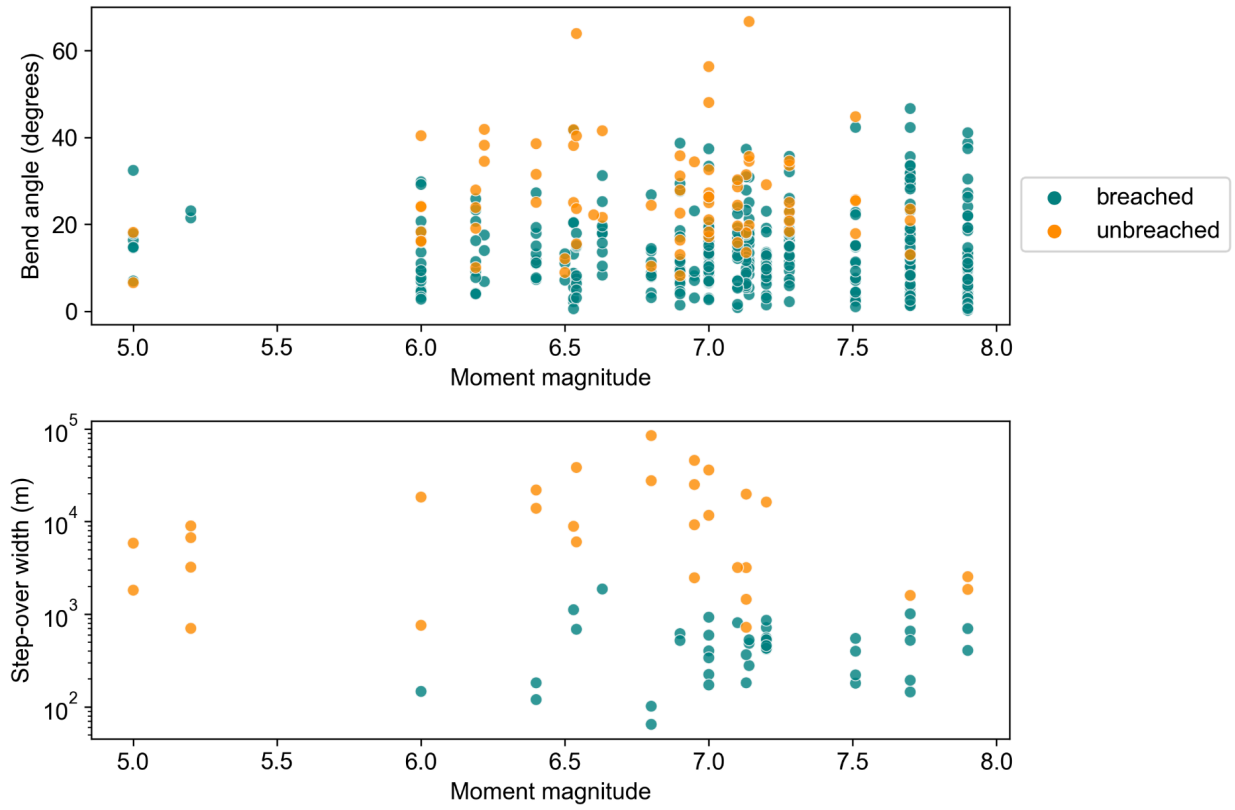

Figure S8. Bend angle (top) and step-over width (bottom) versus event moment magnitude for each of the events considered in this study.

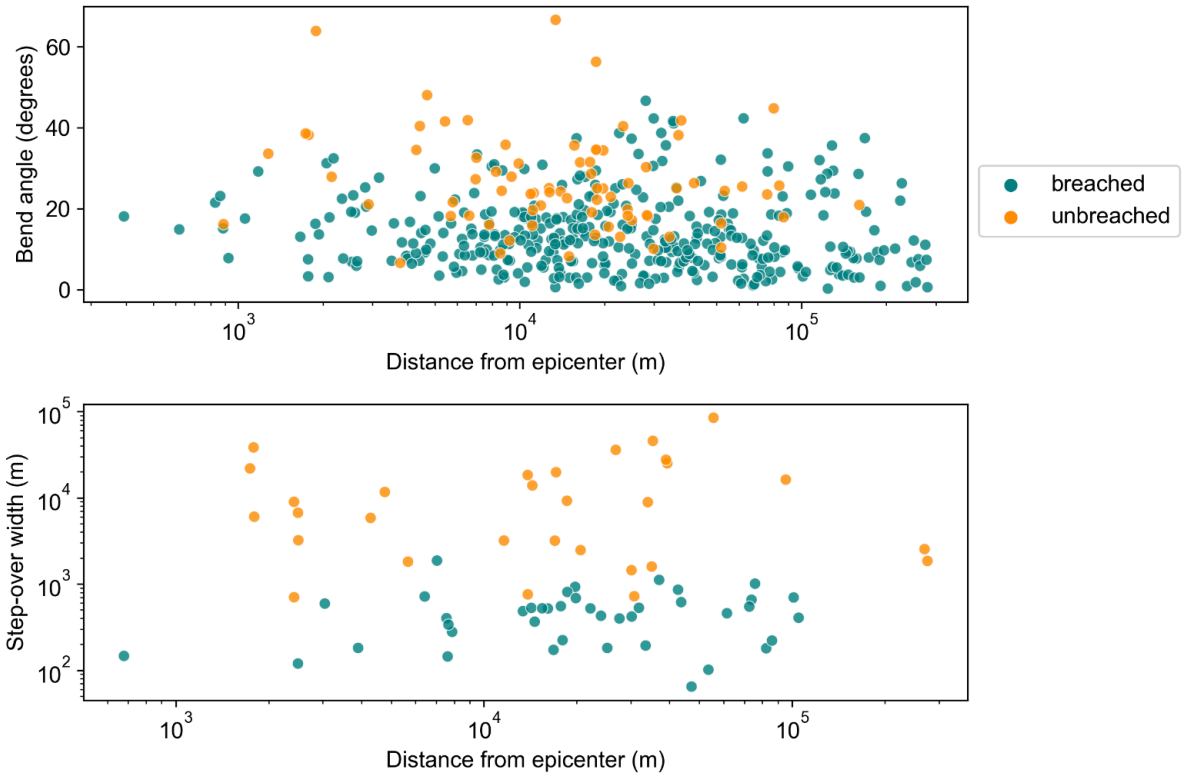

Figure S9. Gate size versus minimum distance to event epicenter. The event epicenters are sourced from the FDHI database (Sarmiento et al. (2021). Note some epicenters in the database are off-fault.

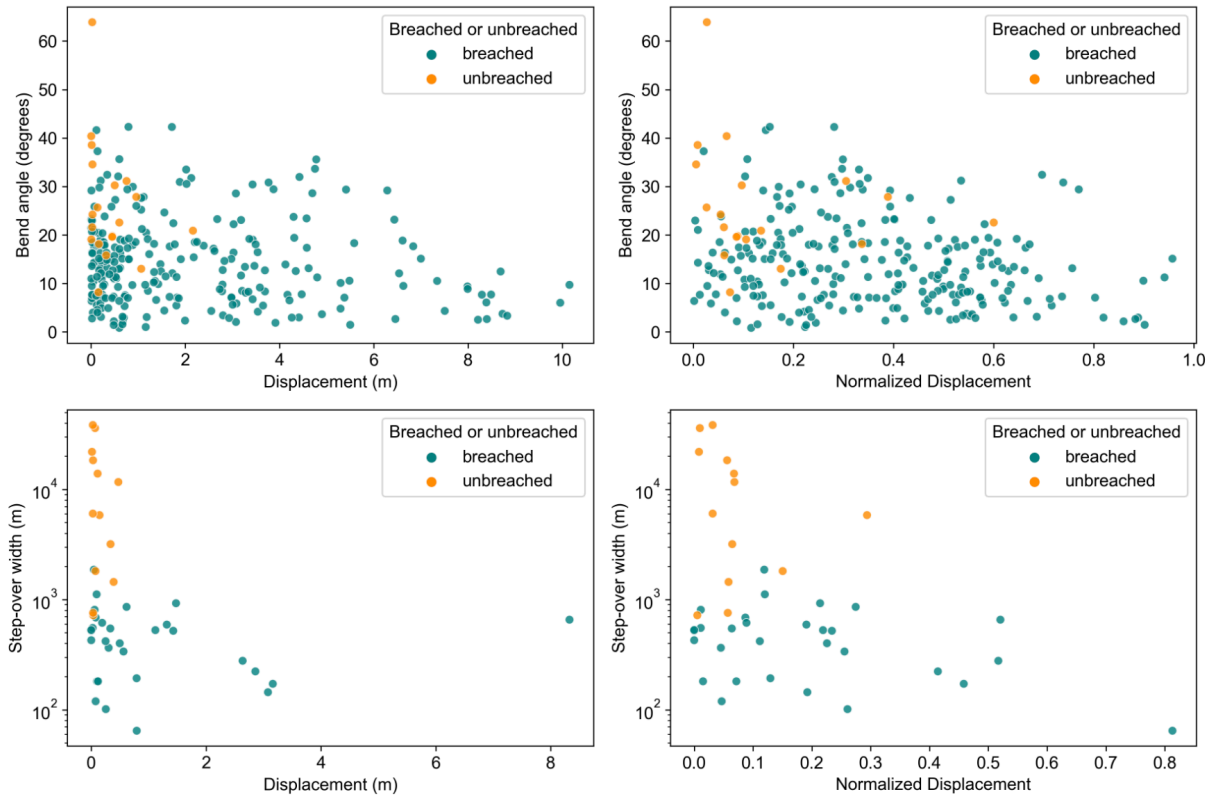

Figure S10. Average slip at bends (top), including both single and double bends, and step-overs (bottom) as a function of bend angle and step-over width. The slip is computed as the average value for all slip measurements available within 500 meters of the earthquake gate. The plots on the left have the mean slip and the ones on the right have the mean slip normalized by the maximum slip of the event the gate was measured for.

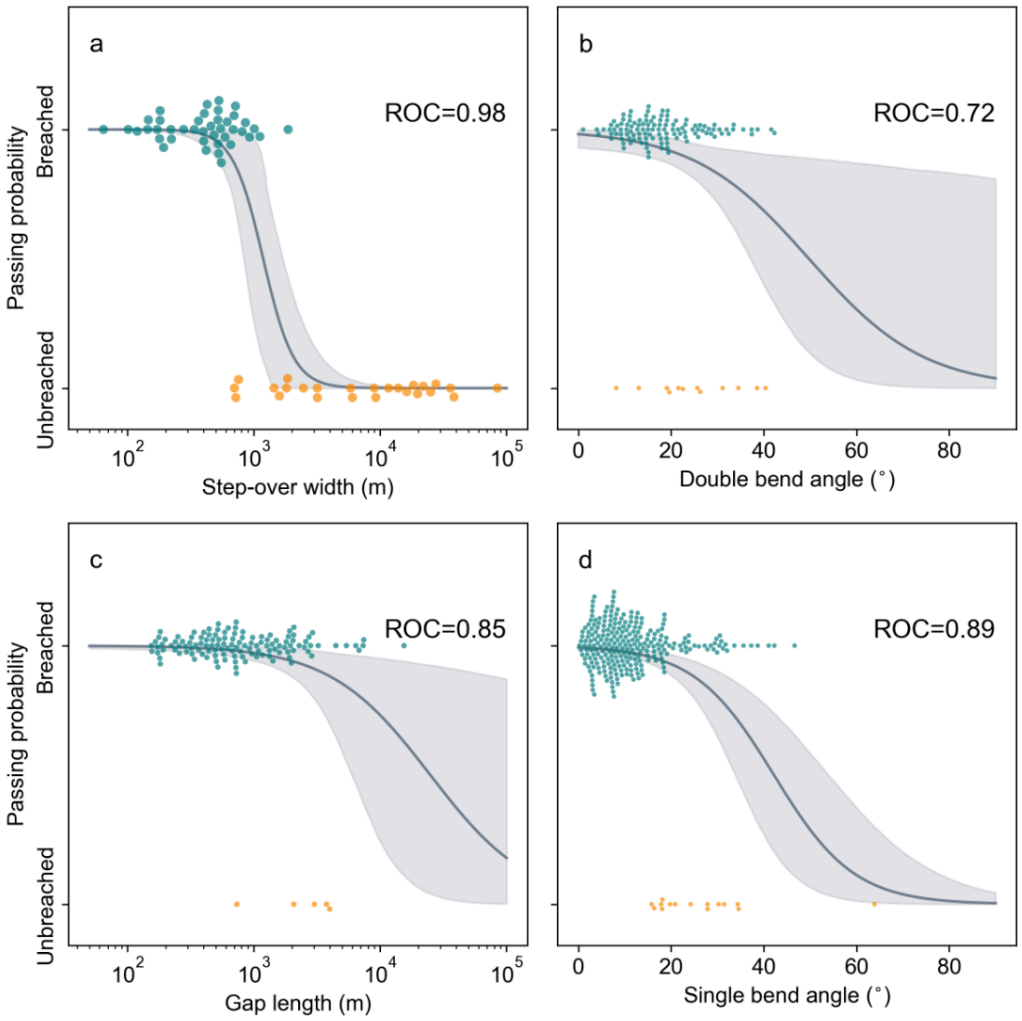

Figure S11. Passing probabilities as a function of geometry including only unbreached earthquake gates at rupture termini (within 5% of the rupture length of each termini). All breached gates are included.

208

Reference Fault Map	Location	References
Quaternary Fault and Fold Database of the United States	United States	USGS and CGS
New Zealand Active Faults Database (NZAFD)	New Zealand	Langridge et al. (2016)
The Active Faults of Eurasia Database (AFEAD)	Europe and Asia	Bachmanov et al. (2021)
GEM Global Active Faults Database	Central and South America	Styron and Pagani (2020)

209

210 **Table S12.** Reference maps of active faults to measure unbreached feature characteristics with
211 respect to.

1 Number of mapped features

Feature	Number mapped
Step-overs	71
Releasing step-overs	26
Restraining step-overs	45
Bends	449
Single bends	297
Double bends	152
Releasing double bends	80
Restraining double bends	72
Gaps	130
Splays	47
Strands	7

2 p-values from the ks tests

Feature A	Feature B	p-value from ks test
Breached double bend	Unbreached double bend	5.049231e-03
Breached single bend	Unbreached single bend	2.679407e-17
Breached step-over	Unbreached step-over	2.340031e-14
Breached gaps	Unbreached gaps	1.418856e-02
Breached splay	Unbreached splay	6.938317e-01
Releasing unbreached bend	Restraining unbreached bend	7.370006e-01
Releasing breached bend	Restraining breached bend	1.402596e-01
Releasing breached step-over	Restraining breached step-over	4.827584e-01
Releasing unbreached step-over	Restraining unbreached step-over	6.820546e-01

3 Passing probabilities from the logistic regressions

Feature	Closest geometry to passing probability = 50%	Units
Double bends	38	degrees
Single bends	32	degrees
Step-overs	1170	meters
Gaps	24500	meters

4 Passing probability on straight section

Feature	Passing probability per meter	Stopping probability per meter
Straight segment	0.99999	0.00001

Event	Termini on straight segments/Total termini	Features at termini
1. Parkfield 1966	1/2	Bend
2. Izmit-Kocaeli	1/2	Bend
3. Landers	4/6	Bends
4. Hector Mine	0/3	Bends, step-overs, gap
5. Balochistan	1/2	Bend
6. Borrego	1/2	Bend
7. Imperial 1979	1/2	Bends, step-over
8. Superstition Hills	0/2	Step-overs, bends
9. Kobe	0/3	Bends
10. Denali	2/2	-
11. Duzce	0/2	Bends
12. Napa	0/3	Step-over, bends, gap
13. Yushu	0/2	Bends
14. Hualien	0/2	Bends
15. Darfield	0/2	Step-overs, bend
16. Galway Lake	0/2	Step-overs
17. Chalfant Valley	0/2	Bends
18. Zirkuh	1/2	Step-over
19. Ridgecrest (foreshock)	0/2	Step-overs, bend
20. Kumamoto	1/3	Bends
21. Ridgecrest (mainshock)	0/2	Step-over, bends
22. Imperial 1940	0/2	Step-overs, bends
23. San Miguel	0/2	Step-overs, bend
24. Yutian	1/2	Bend
25. Luzon	0/2	Bends, step-over, gap
26. Elmore Ranch	0/2	Bends
27. Pisayambo	0/2	Step-overs, bends
28. Izu Peninsula	0/2	Bends
29. Izu Oshima	1/2	Bend
30. Neftegorsk	0/2	Bends
31. Parkfield 2004	1/2	Bend
All events	**16/70**	-

Table 1: Number of termini on straight fault segments and on earthquake gates for the events on the FDHI database.

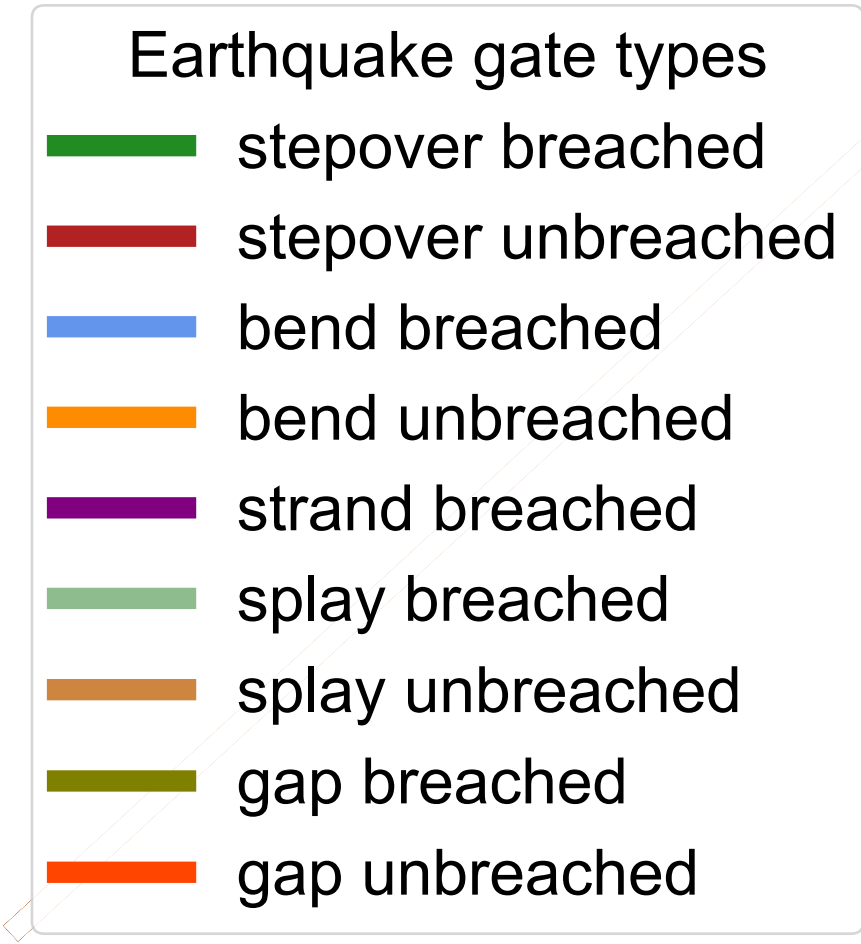
Earthquake gate types
stepover breached
stepover unbreached
bend breached
bend unbreached
strand breached
splay breached
splay unbreached
gap breached
gap unbreached

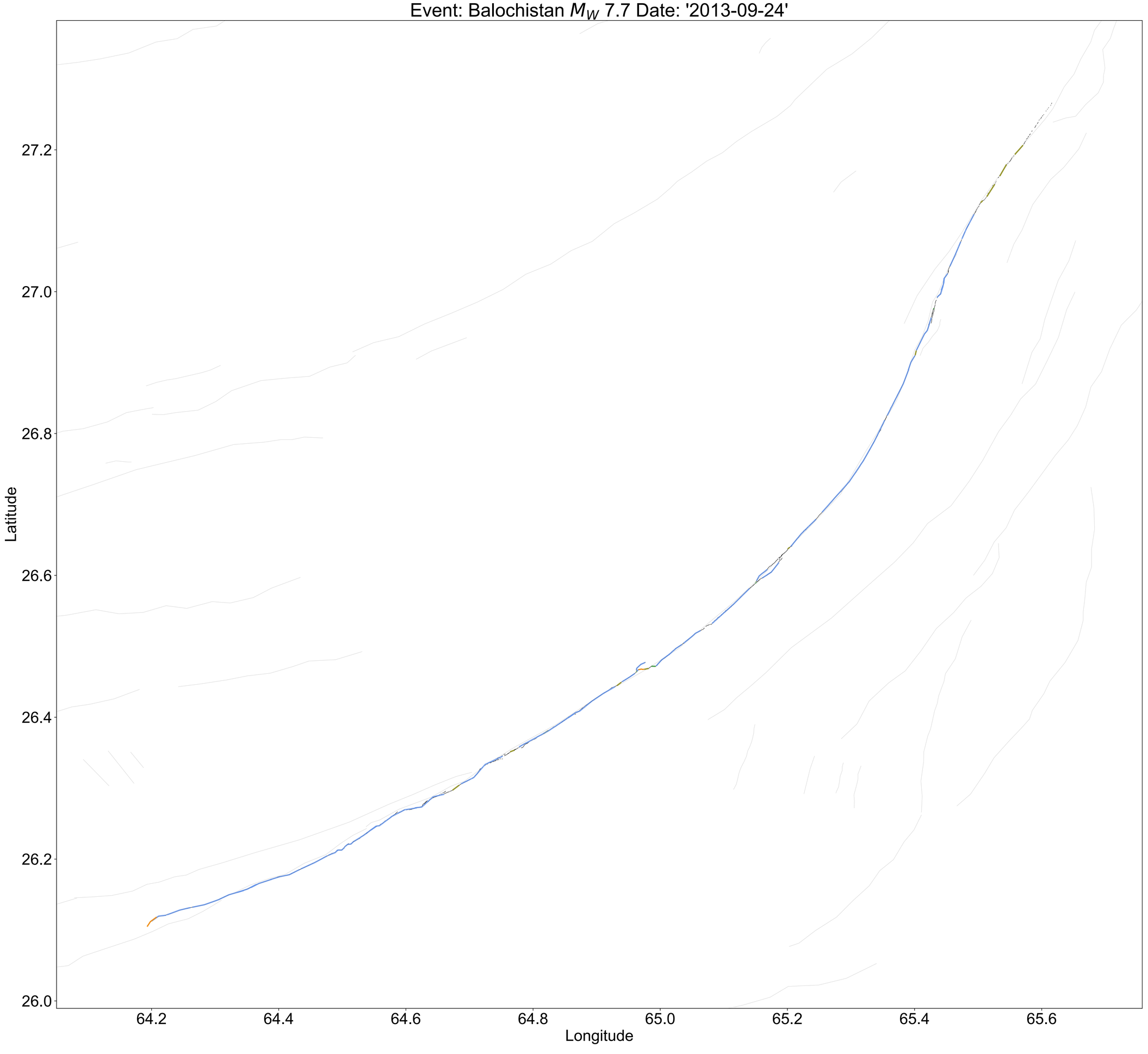
Event: Balochistan M_W 7.7 Date: '2013-09-24'
Latitude
27.2
27.0
26.8
26.6
26.4
26.2
26.0
64.2
64.4
64.6
64.8
65.0
65.2
65.4
65.6
Longitude

Event: Borrego M_W 6.63 Date: '1968-04-09'

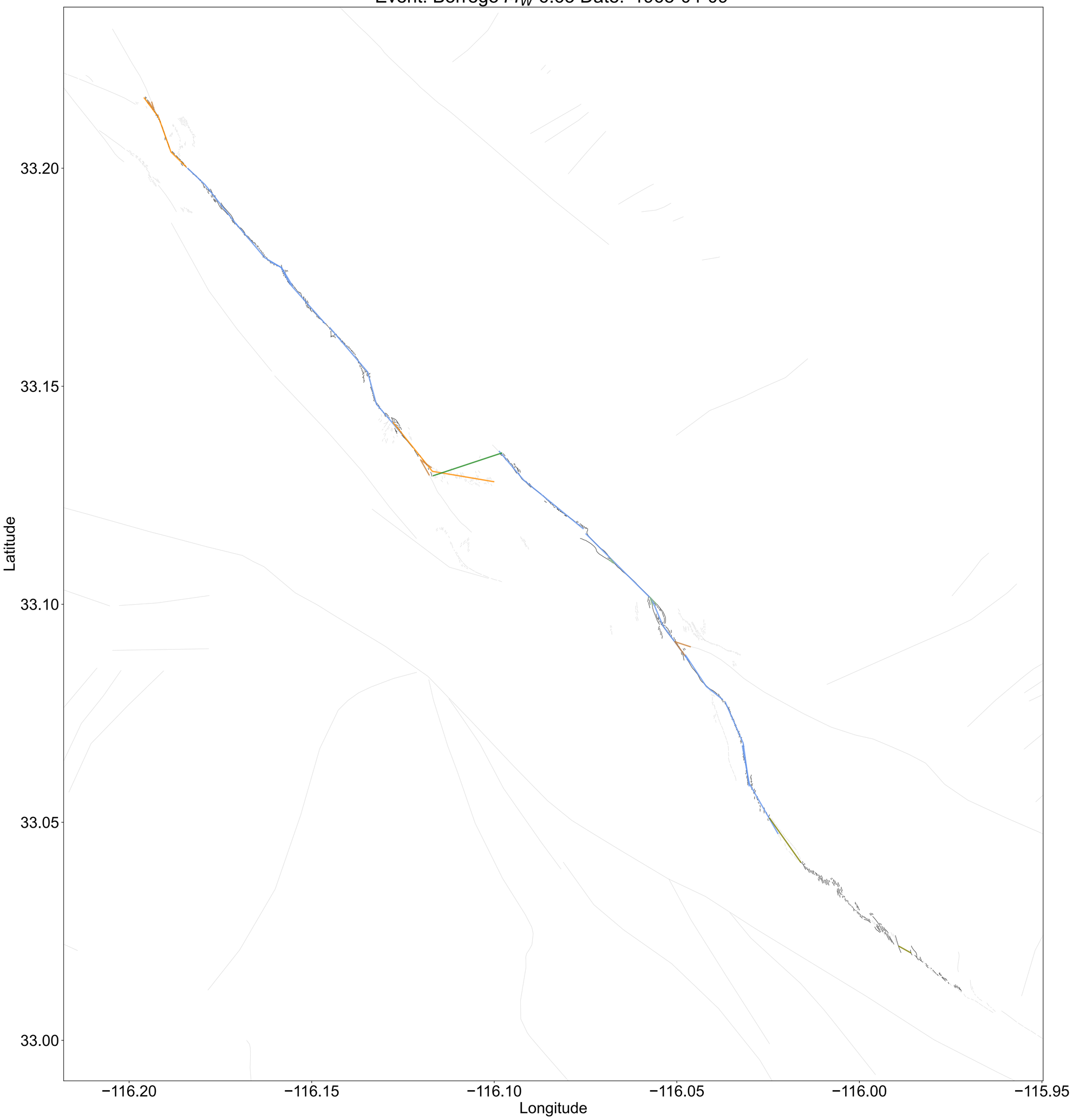

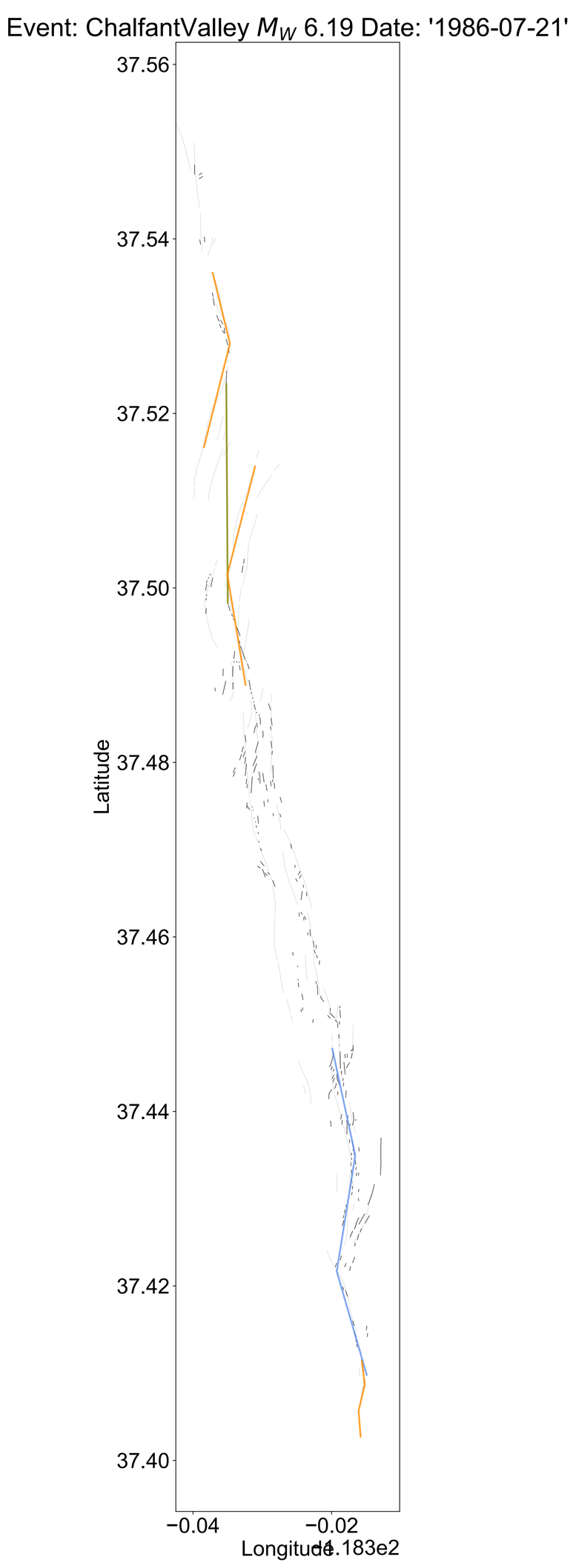
Event: ChalfantValley M_W 6.19 Date: '1986-07-21'
37.56
37.54
37.52
37.50
37.48
37.46
37.44
37.42
37.40
Latitude
−0.04
−0.02
Longitude
+4.183e2

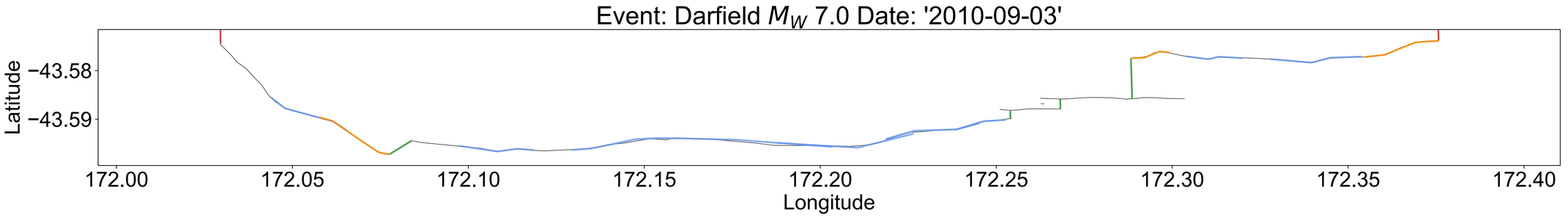
Event: Darfield M_W 7.0 Date: '2010-09-03'
Latitude
−43.58
−43.59
172.00
172.05
172.10
172.15
172.20
172.25
172.30
172.35
172.40
Longitude

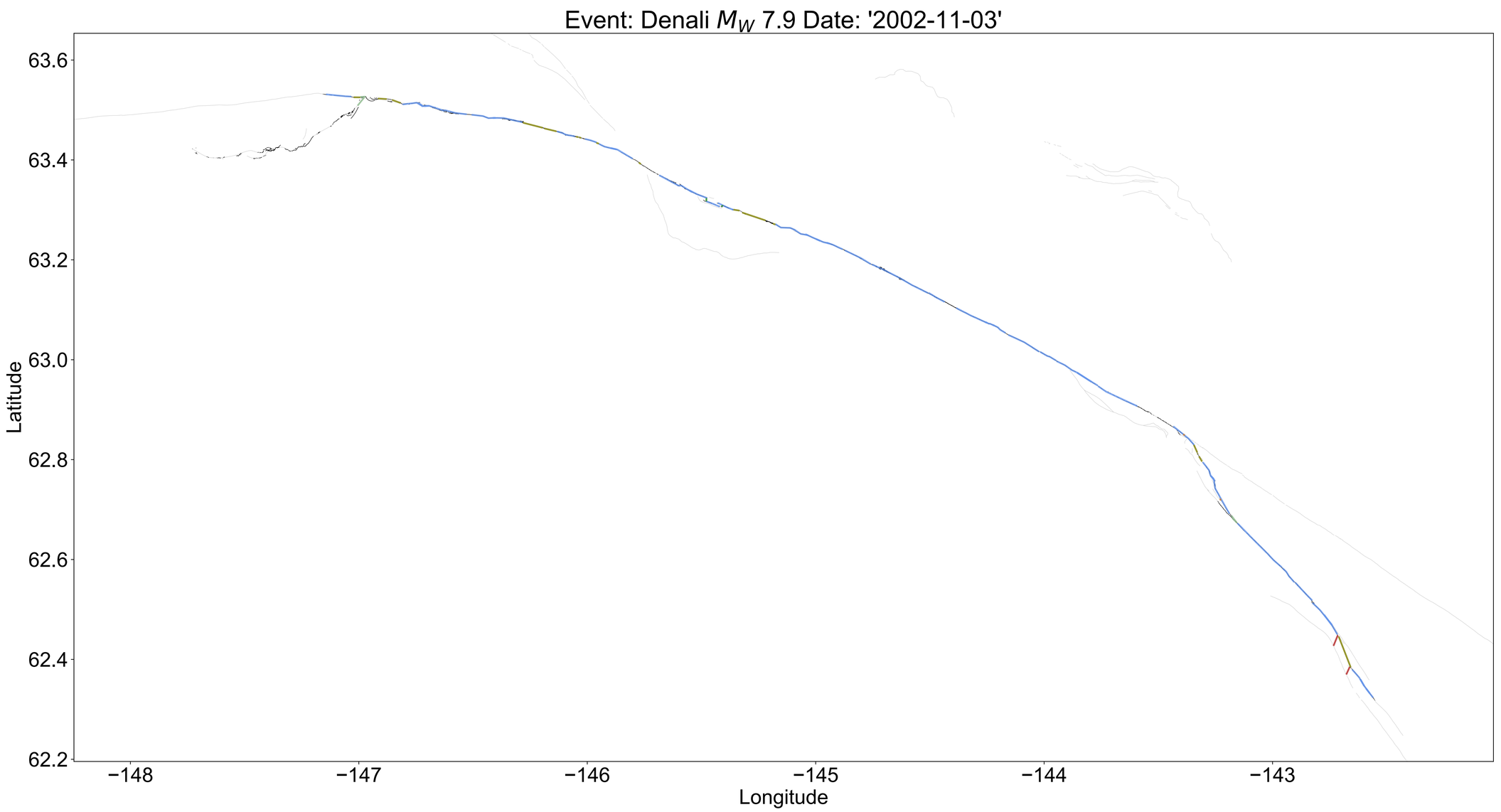
Event: Denali M_W 7.9 Date: '2002-11-03'
63.6
63.4
63.2
63.0
62.8
62.6
62.4
62.2
Latitude
−148
−147
−146
−145
−144
−143
Longitude

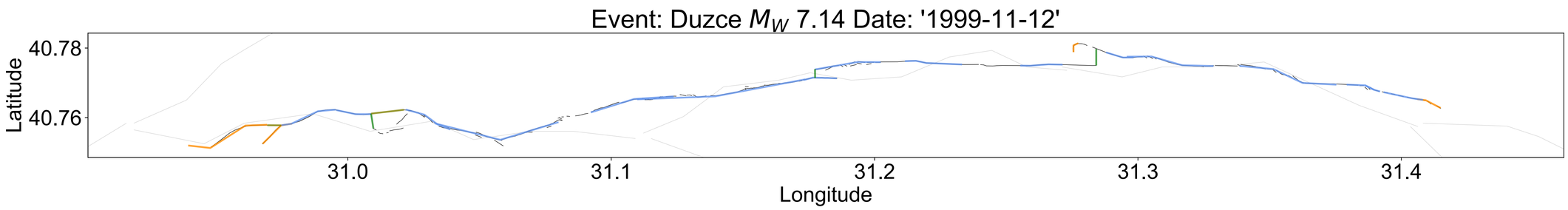
Event: Duzce M_W 7.14 Date: '1999-11-12'
Latitude
40.78
40.76
31.0
31.1
31.2
31.3
31.4
Longitude

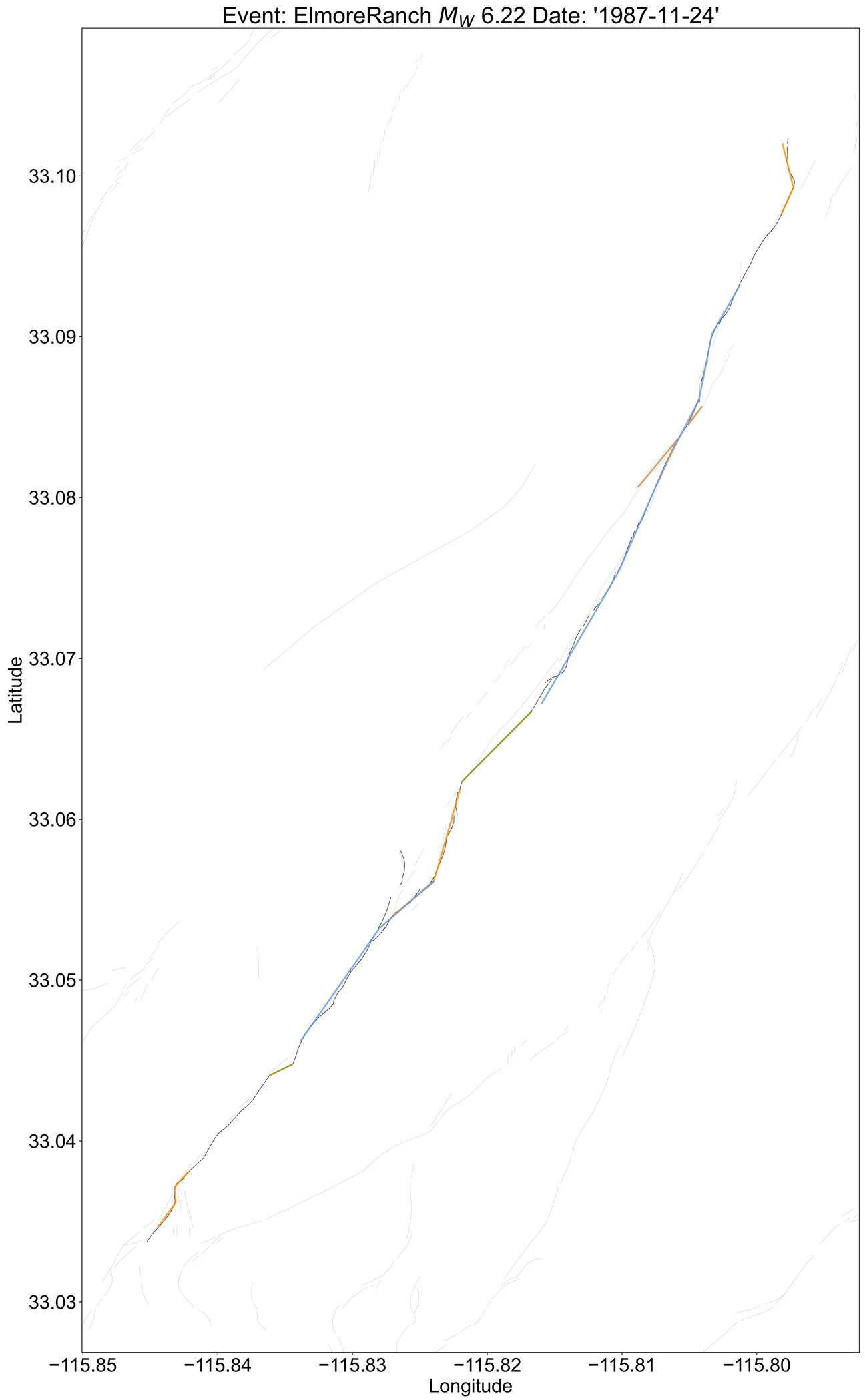
Event: ElmoreRanch M_W 6.22 Date: '1987-11-24'
33.10
33.09
33.08
33.07
33.06
33.05
33.04
33.03
Latitude
−115.85
−115.84
−115.83
−115.82
−115.81
−115.80
Longitude

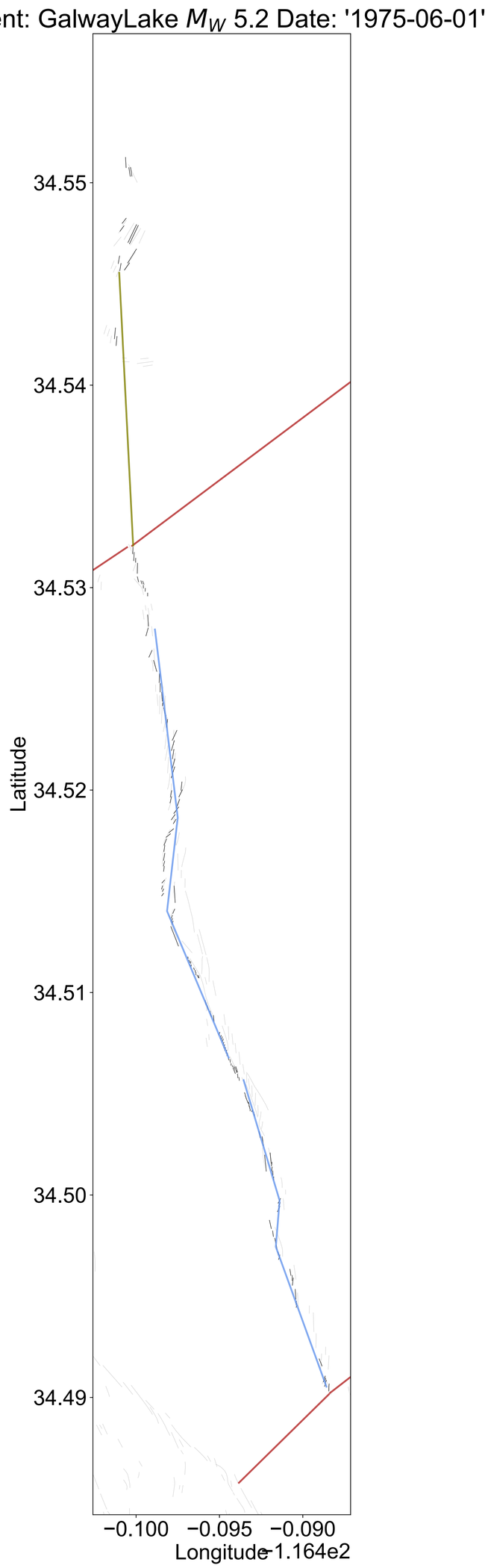
Event: GalwayLake M_W 5.2 Date: '1975-06-01'
34.55
34.54
34.53
34.52
34.51
34.50
34.49
Latitude
−0.100
−0.095
−0.090
−1.164e2
Longitude

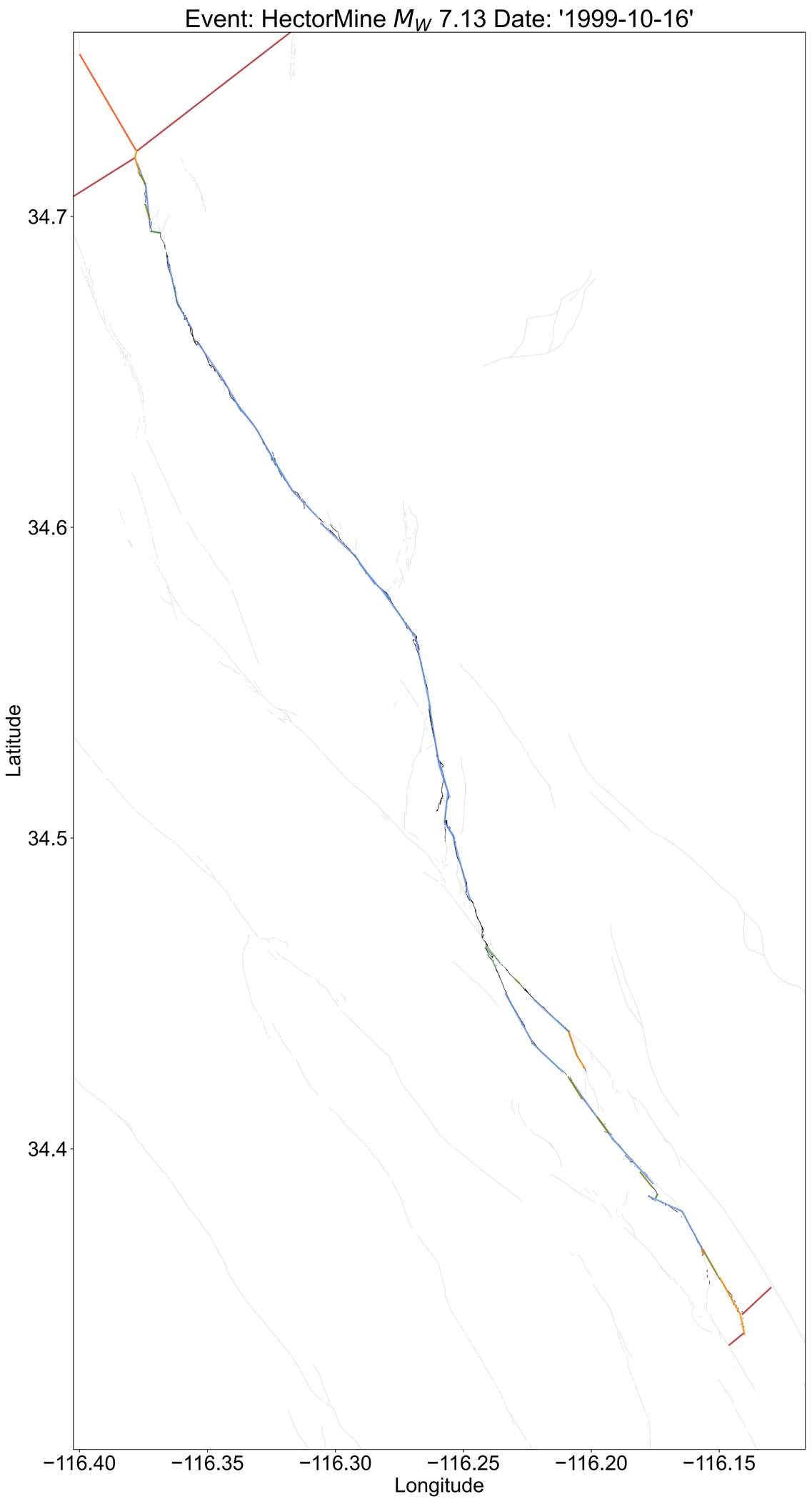
Event: HectorMine M_W 7.13 Date: '1999-10-16'
34.7
34.6
34.5
34.4
Latitude
−116.40
−116.35
−116.30
−116.25
−116.20
−116.15
Longitude

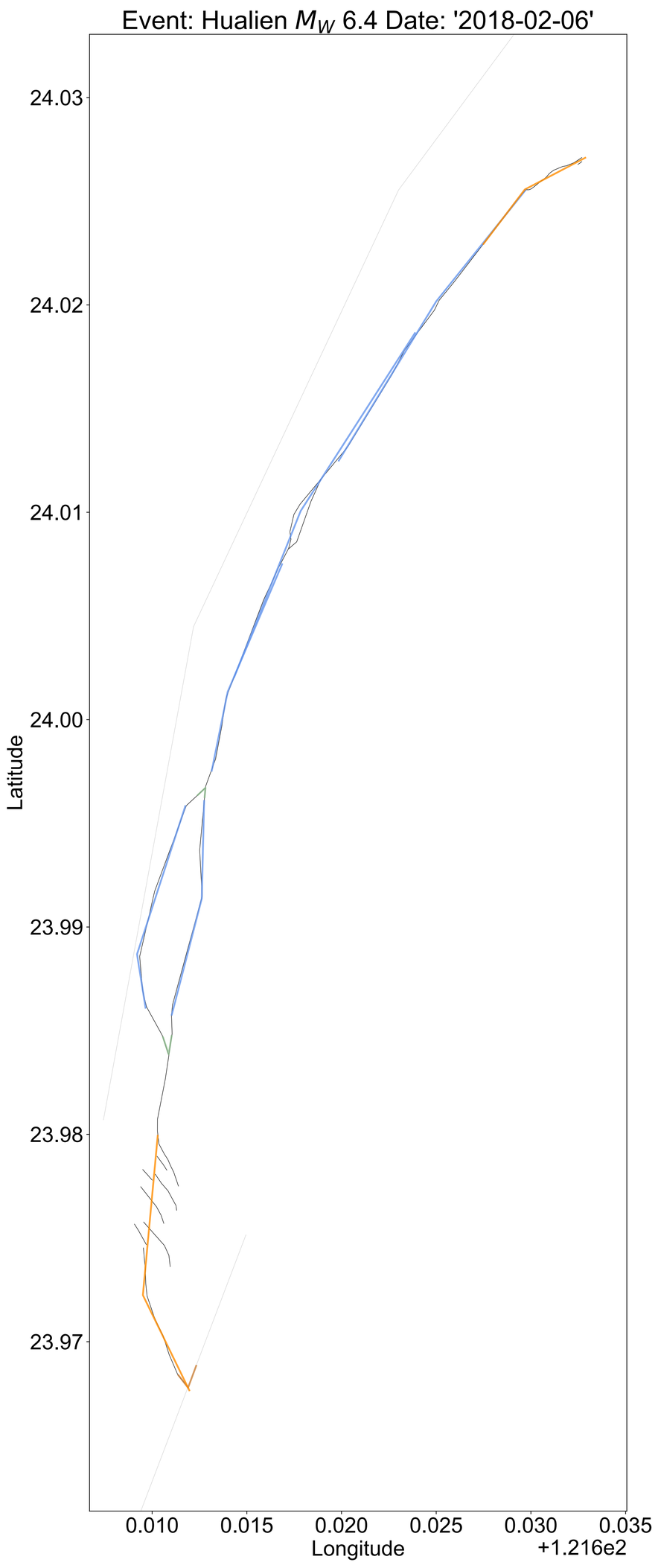
Event: Hualien M_W 6.4 Date: '2018-02-06'
24.03
24.02
24.01
24.00
23.99
23.98
23.97
Latitude
0.010
0.015
0.020
0.025
0.030
0.035
Longitude
+1.216e2

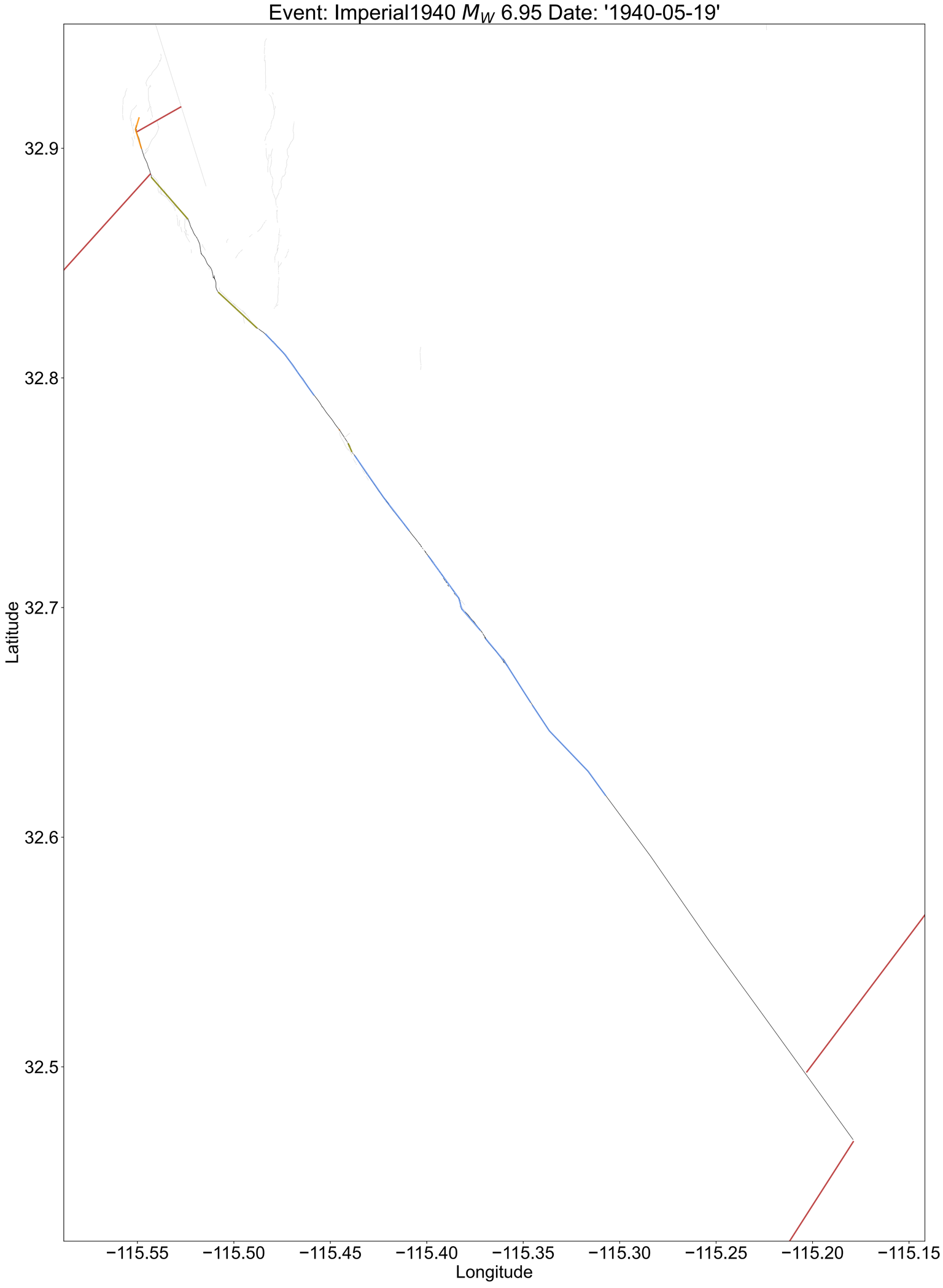
Event: Imperial1940 M_W 6.95 Date: '1940-05-19'
32.9
32.8
32.7
32.6
32.5
Latitude
−115.55
−115.50
−115.45
−115.40
−115.35
−115.30
−115.25
−115.20
−115.15
Longitude

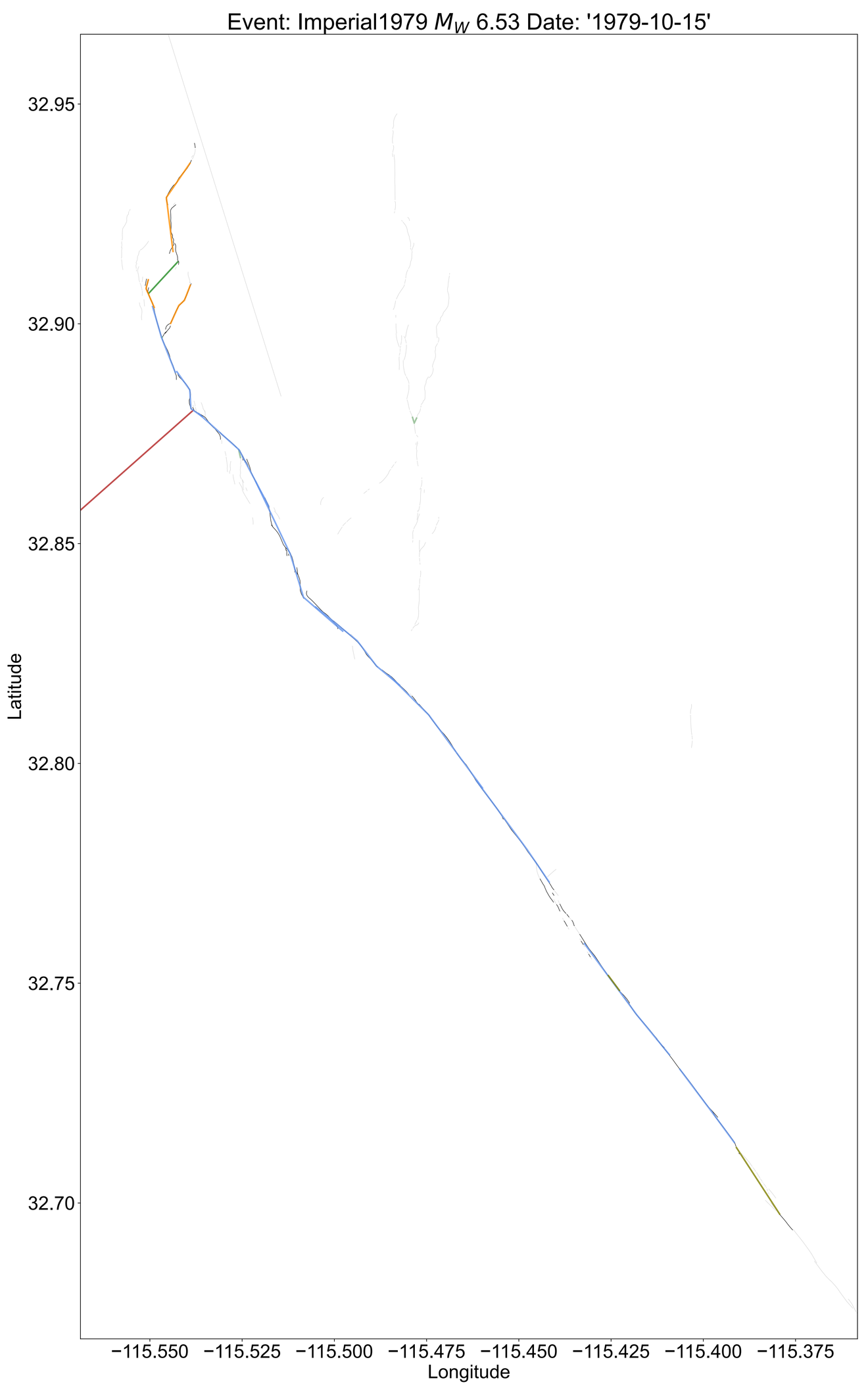
Event: Imperial1979 M_W 6.53 Date: '1979-10-15'
32.95
32.90
32.85
32.80
32.75
32.70
Latitude
−115.550
−115.525
−115.500
−115.475
−115.450
−115.425
−115.400
−115.375
Longitude

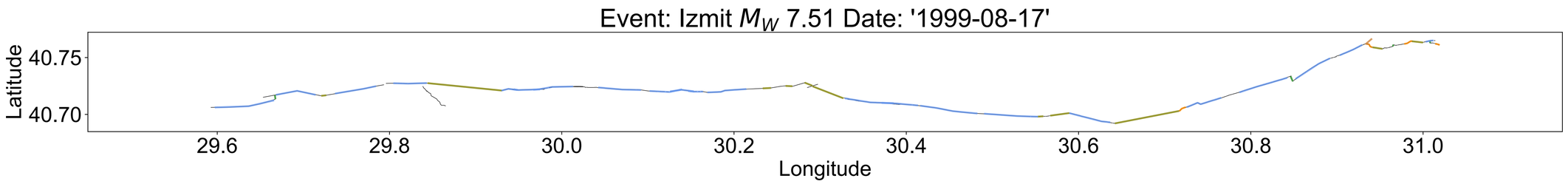
Event: Izmit M_W 7.51 Date: '1999-08-17'
Latitude
40.75
40.70
29.6
29.8
30.0
30.2
30.4
30.6
30.8
31.0
Longitude

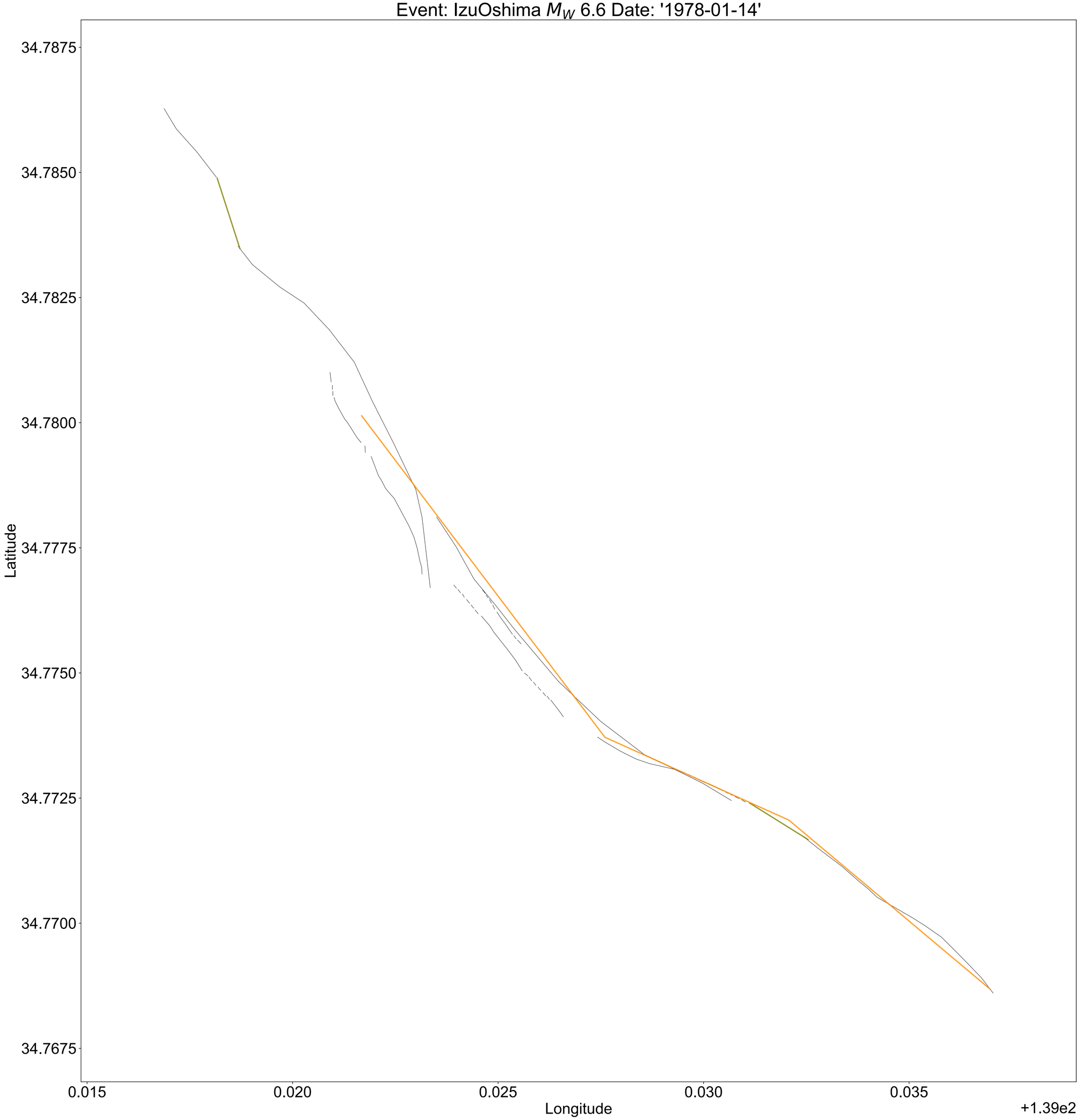
Event: IzuOshima M_W 6.6 Date: '1978-01-14'
34.7875
34.7850
34.7825
34.7800
34.7775
34.7750
34.7725
34.7700
34.7675
Latitude
0.015
0.020
0.025
0.030
0.035
+1.39e2
Longitude

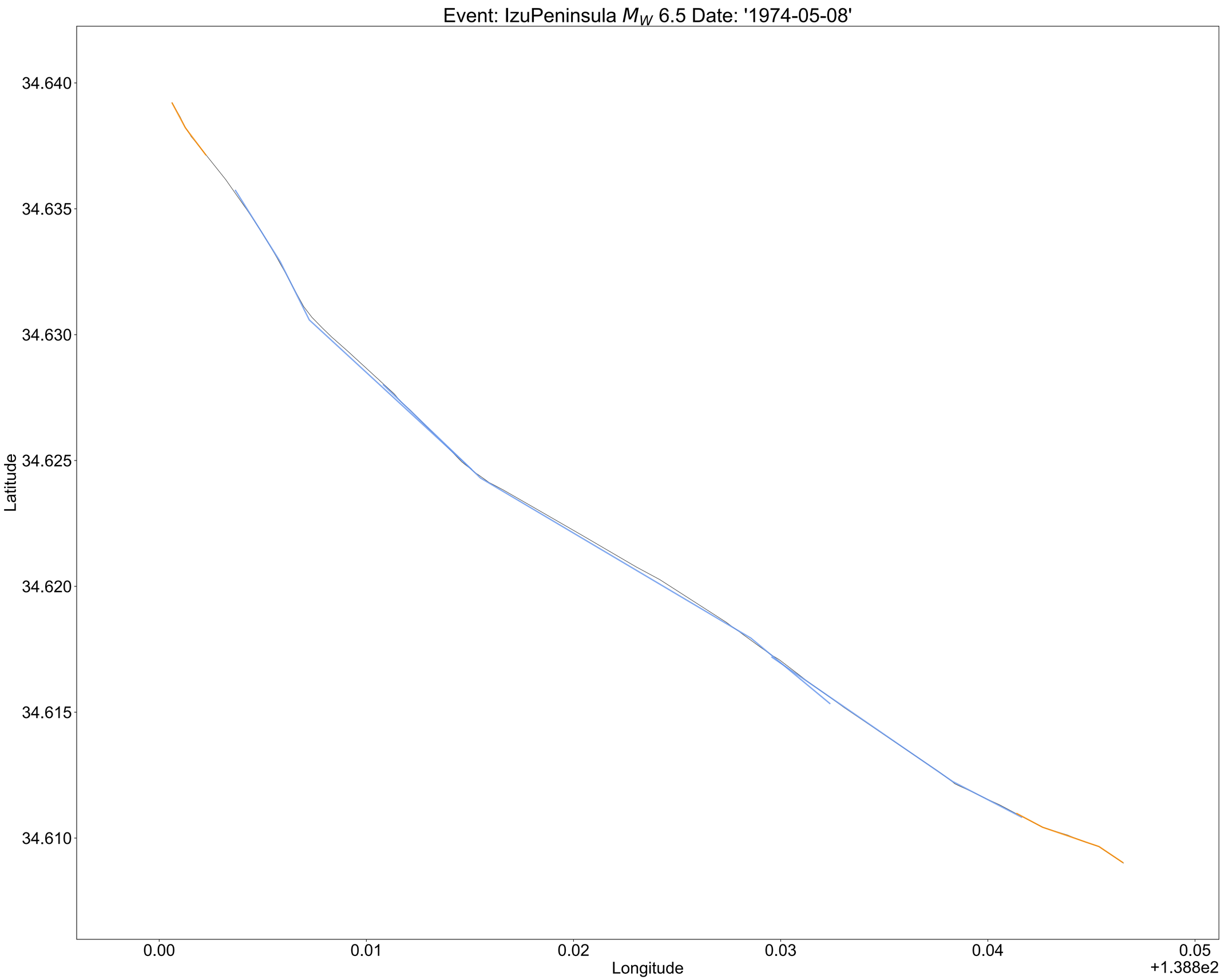
Event: IzuPeninsula M_W 6.5 Date: '1974-05-08'
34.640
34.635
34.630
34.625
34.620
34.615
34.610
Latitude
0.00
0.01
0.02
0.03
0.04
0.05
+1.388e2
Longitude

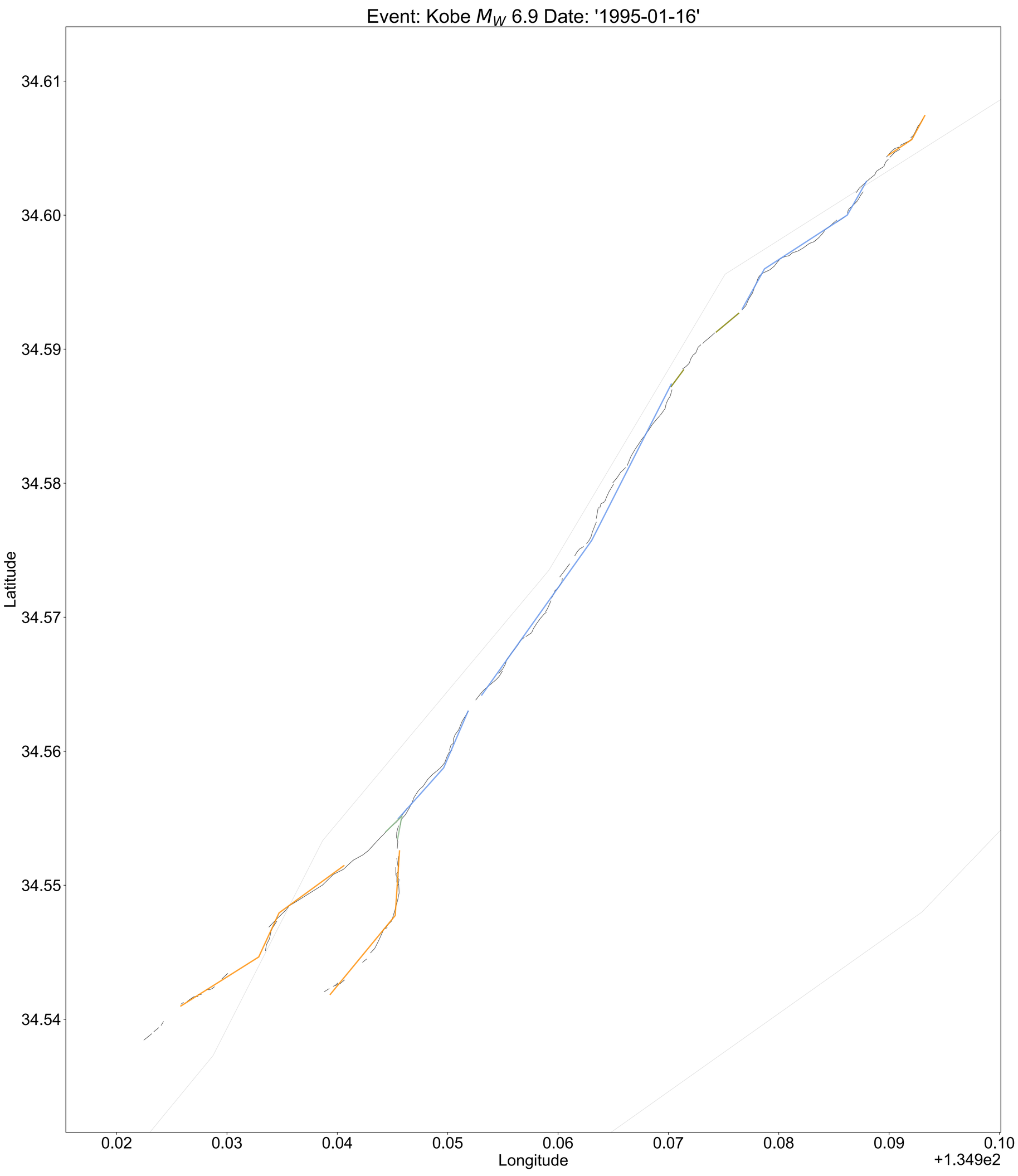
Event: Kobe M_W 6.9 Date: '1995-01-16'
Latitude
34.61
34.60
34.59
34.58
34.57
34.56
34.55
34.54
0.02
0.03
0.04
0.05
0.06
0.07
0.08
0.09
0.10
Longitude
+1.349e2

Event: Kumamoto M_W 7.0 Date: '2016-04-15'

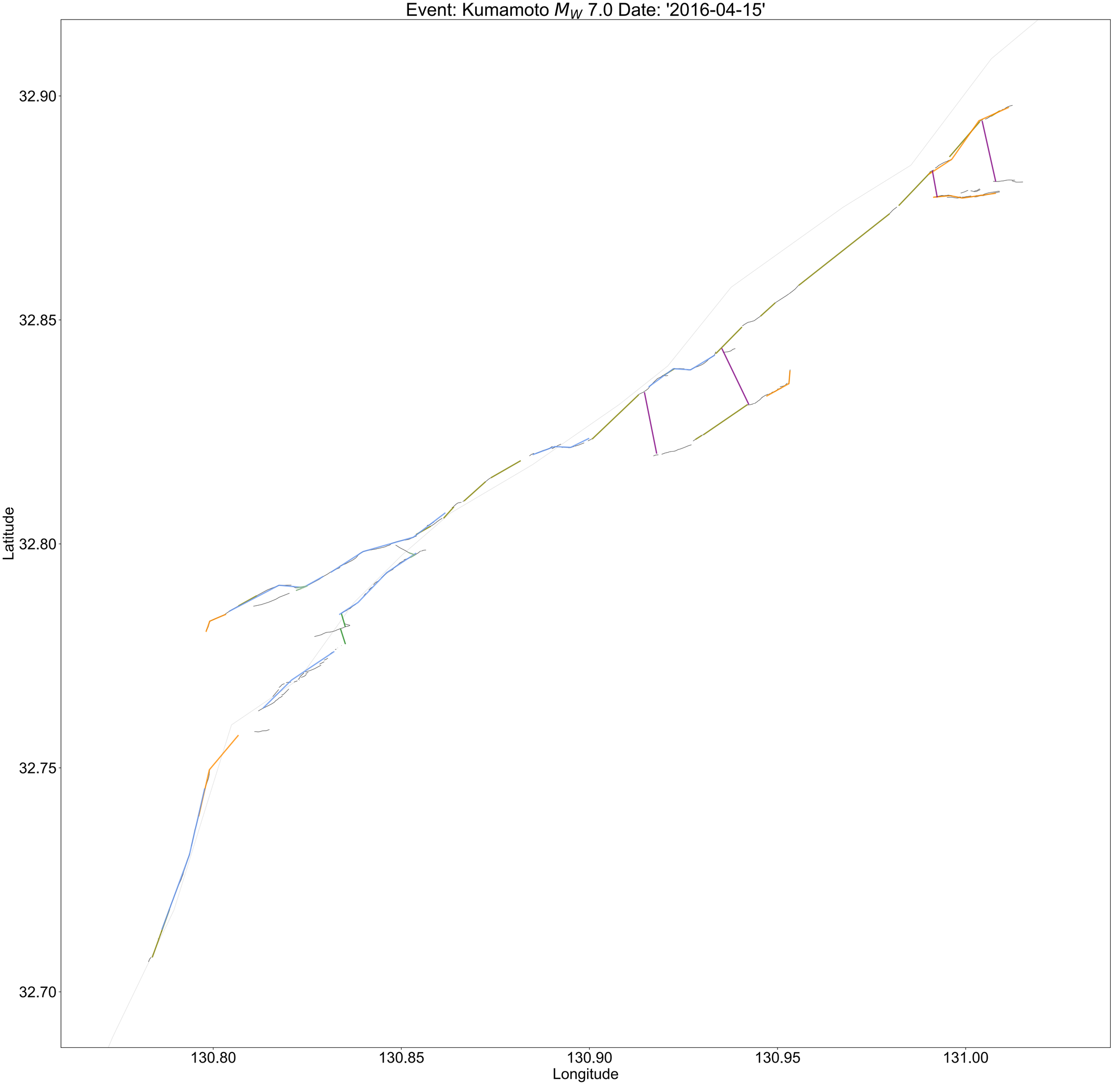

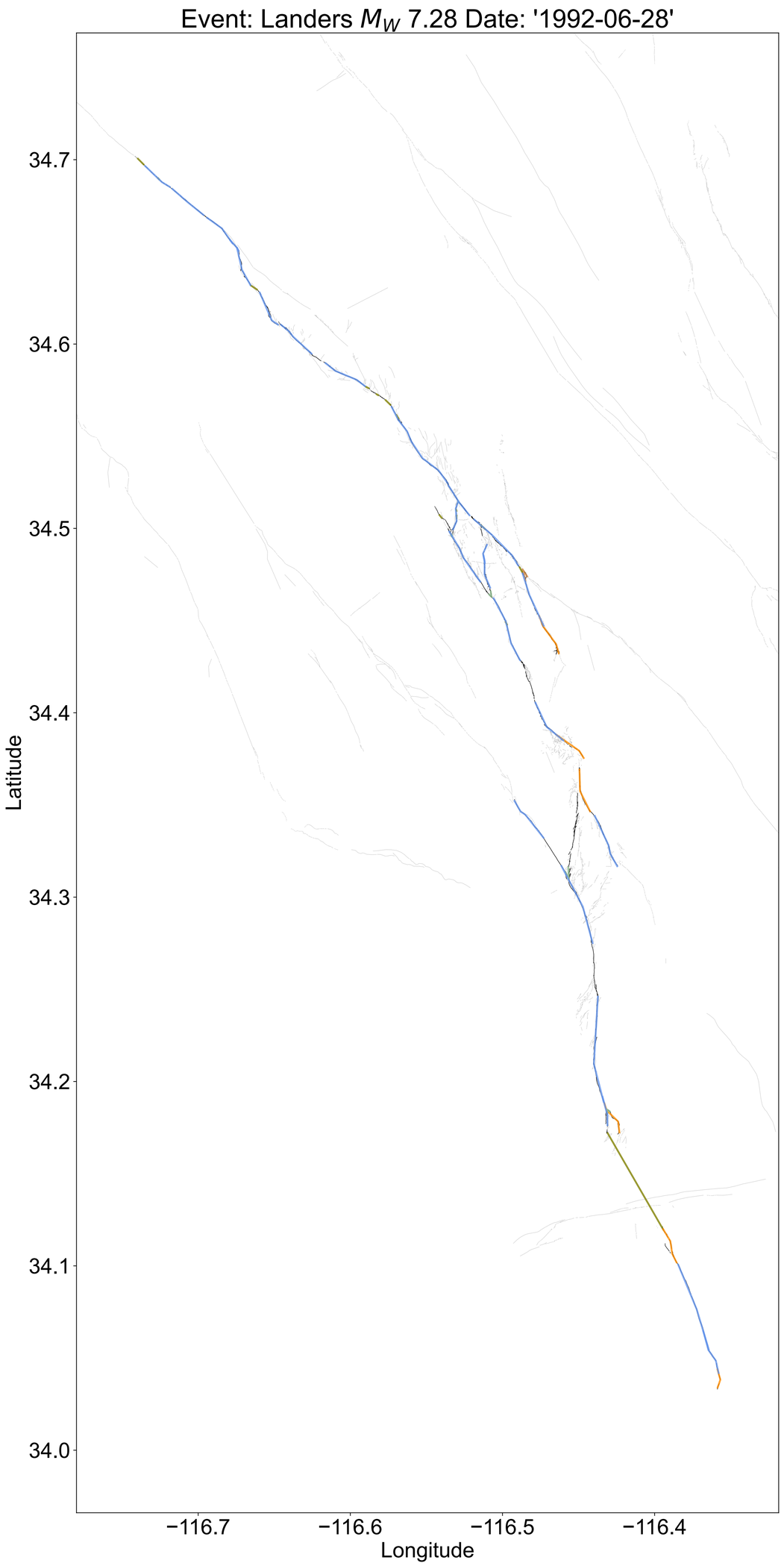
Event: Landers M_W 7.28 Date: '1992-06-28'
34.7
34.6
34.5
34.4
34.3
34.2
34.1
34.0
Latitude
−116.7
−116.6
−116.5
−116.4
Longitude

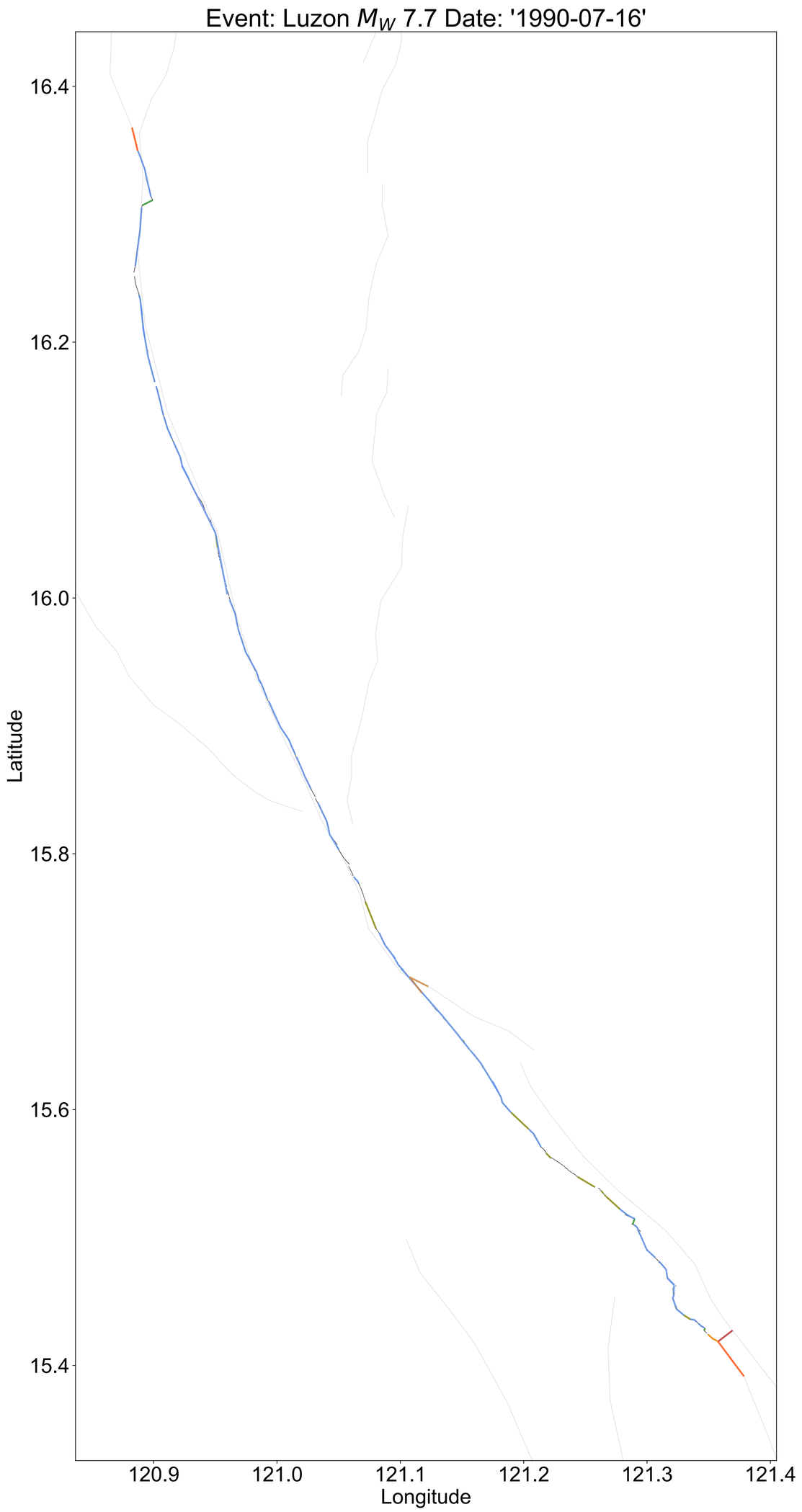
Event: Luzon M_W 7.7 Date: '1990-07-16'
16.4
16.2
16.0
15.8
15.6
15.4
Latitude
120.9
121.0
121.1
121.2
121.3
121.4
Longitude

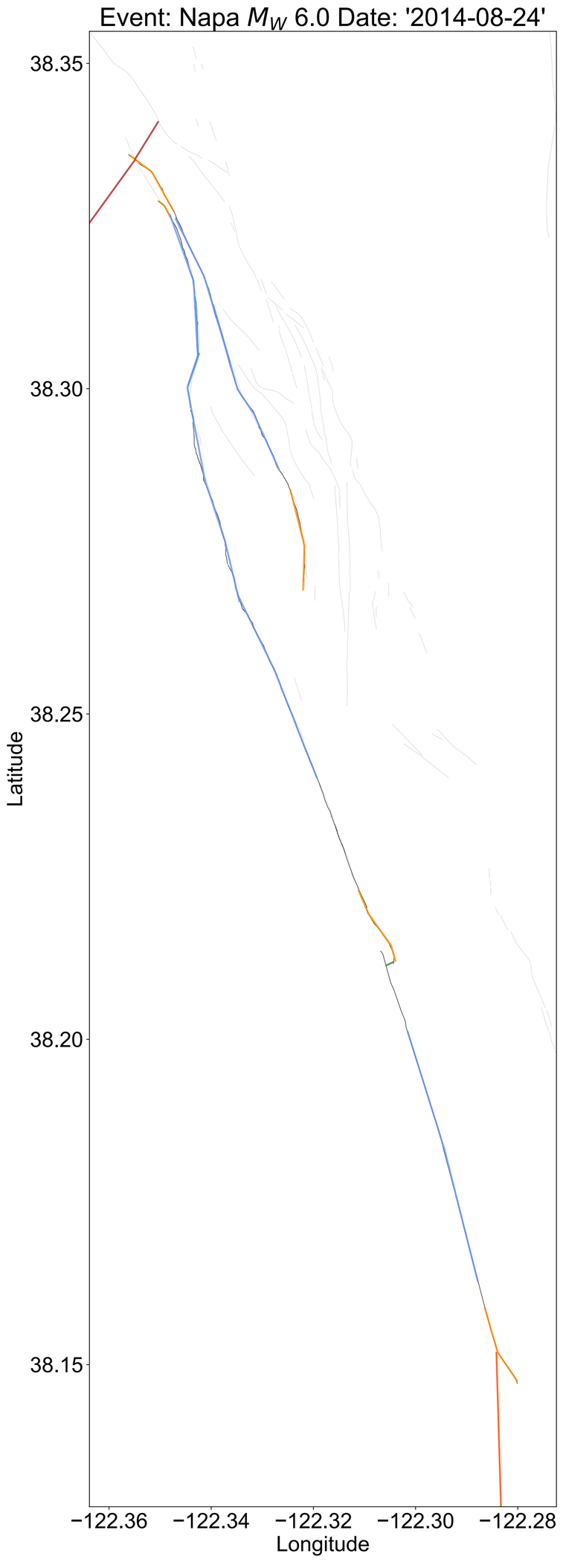
Event: Napa M_W 6.0 Date: '2014-08-24'
38.35
38.30
38.25
38.20
38.15
Latitude
−122.36
−122.34
−122.32
−122.30
−122.28
Longitude

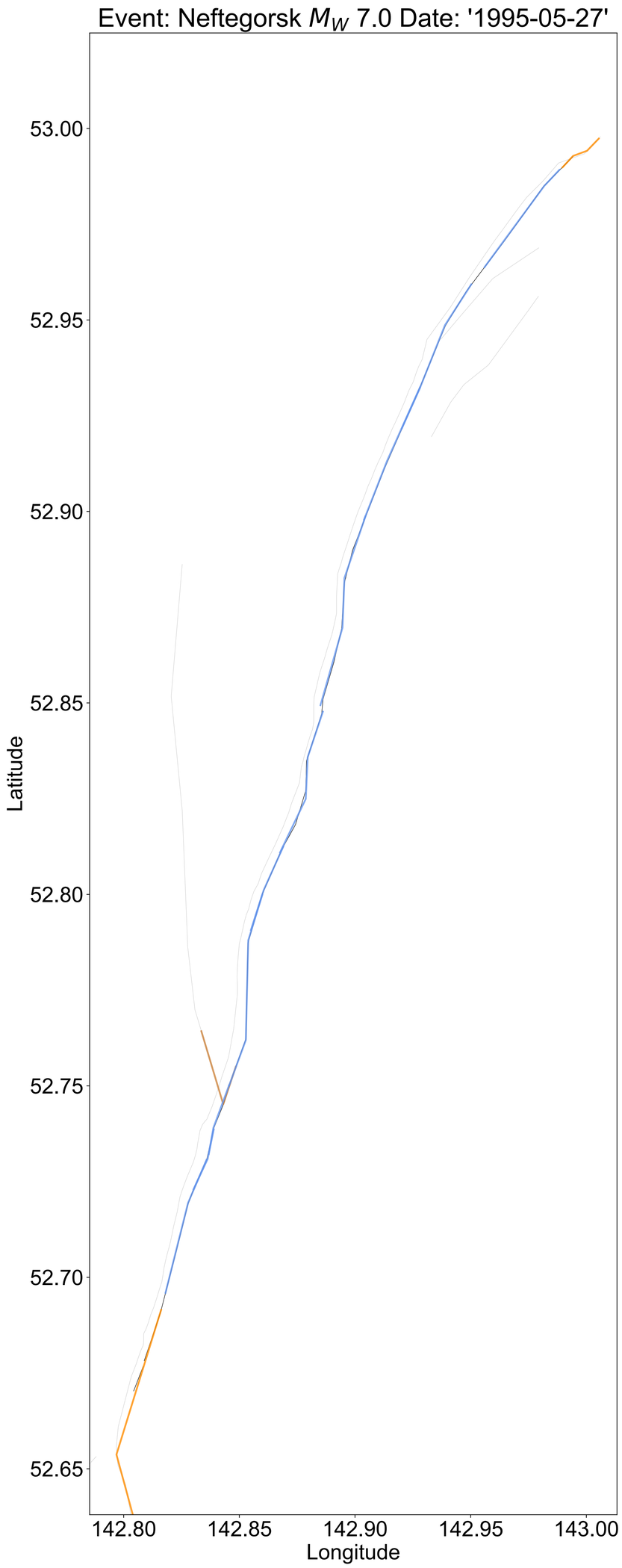
Event: Neftegorsk M_W 7.0 Date: '1995-05-27'
53.00
52.95
52.90
52.85
52.80
52.75
52.70
52.65
Latitude
142.80
142.85
142.90
142.95
143.00
Longitude

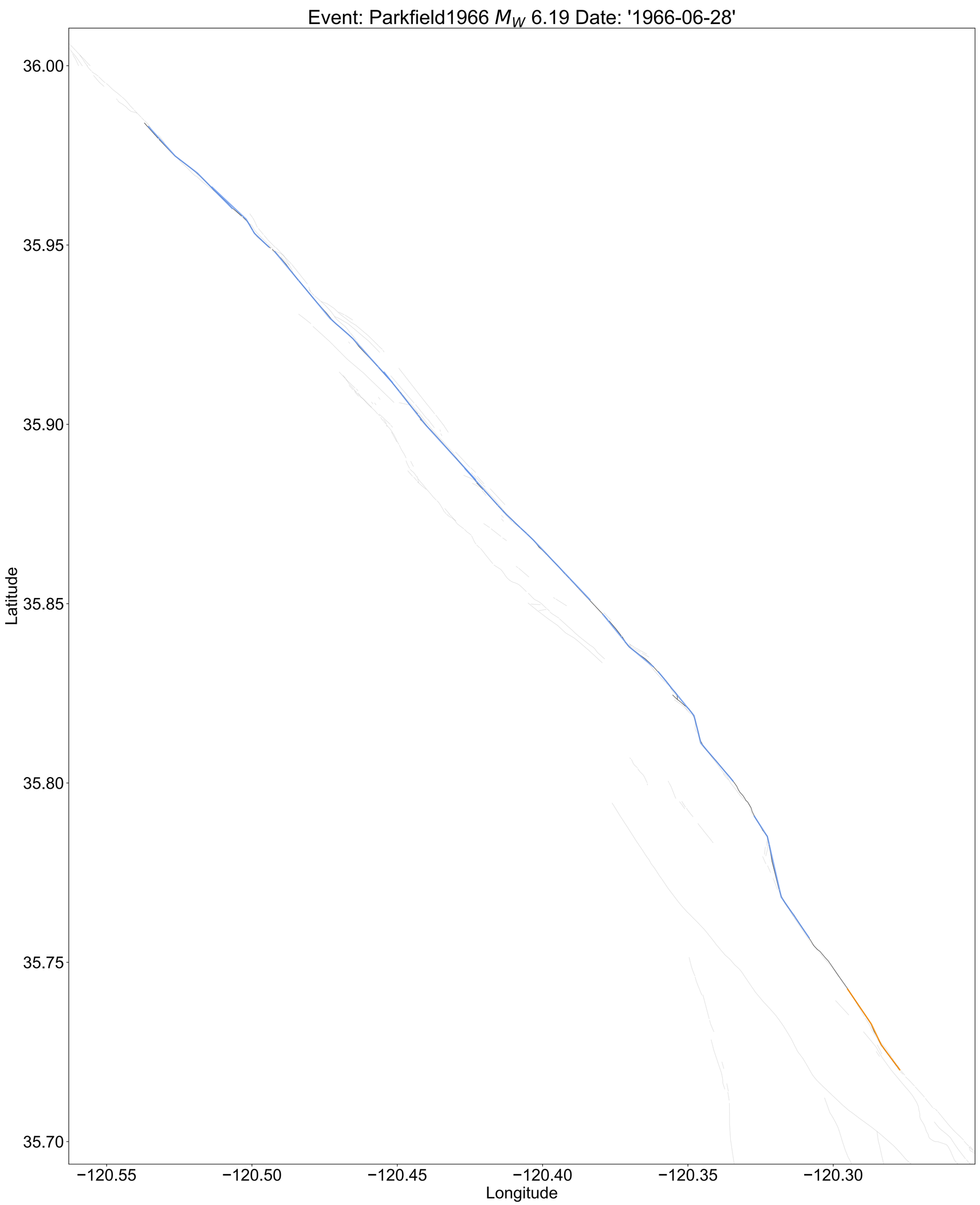
Event: Parkfield1966 M_W 6.19 Date: '1966-06-28'
36.00
35.95
35.90
35.85
35.80
35.75
35.70
Latitude
−120.55
−120.50
−120.45
−120.40
−120.35
−120.30
Longitude

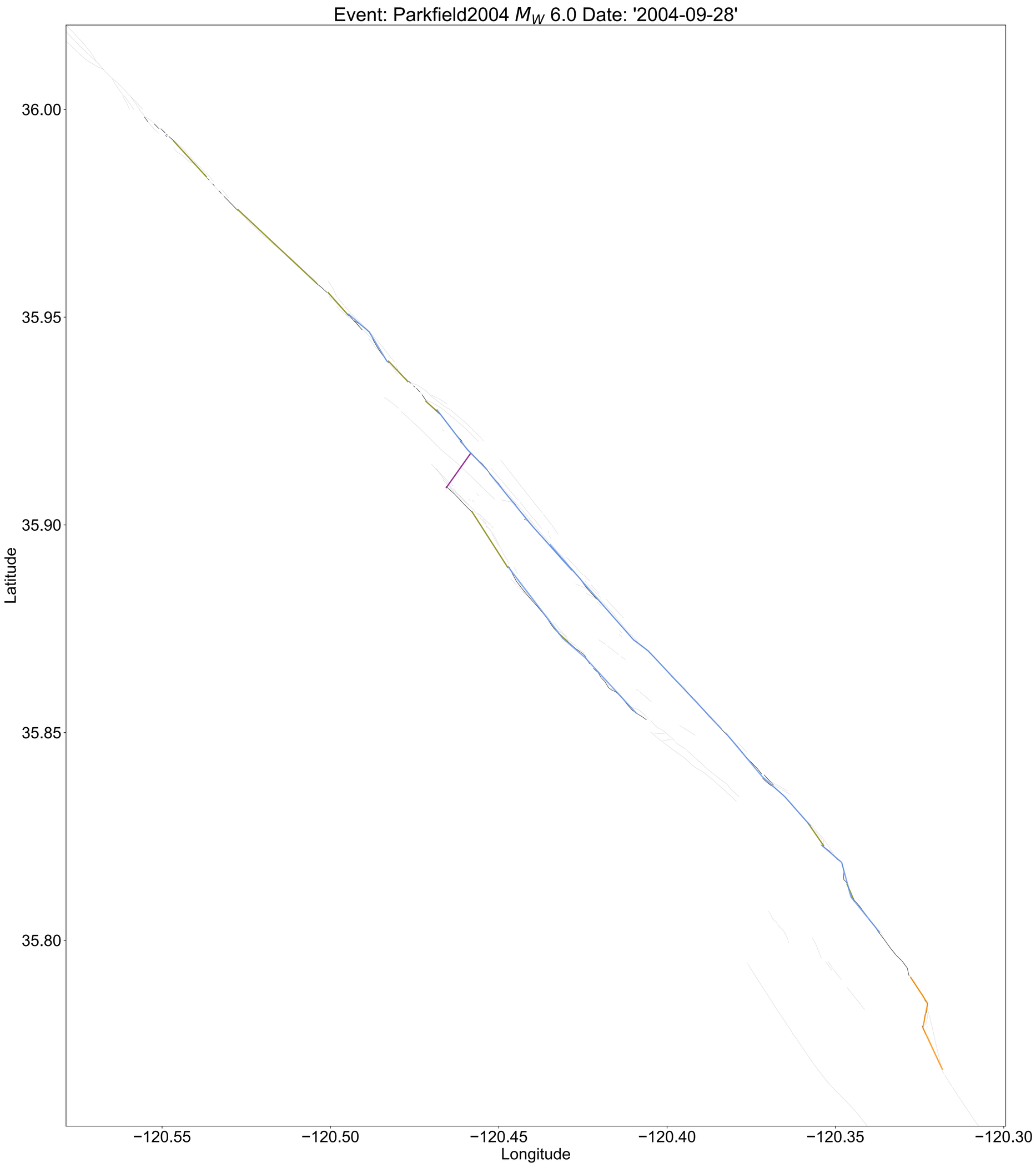
Event: Parkfield2004 M_W 6.0 Date: '2004-09-28'
36.00
35.95
35.90
35.85
35.80
Latitude
−120.55
−120.50
−120.45
−120.40
−120.35
−120.30
Longitude

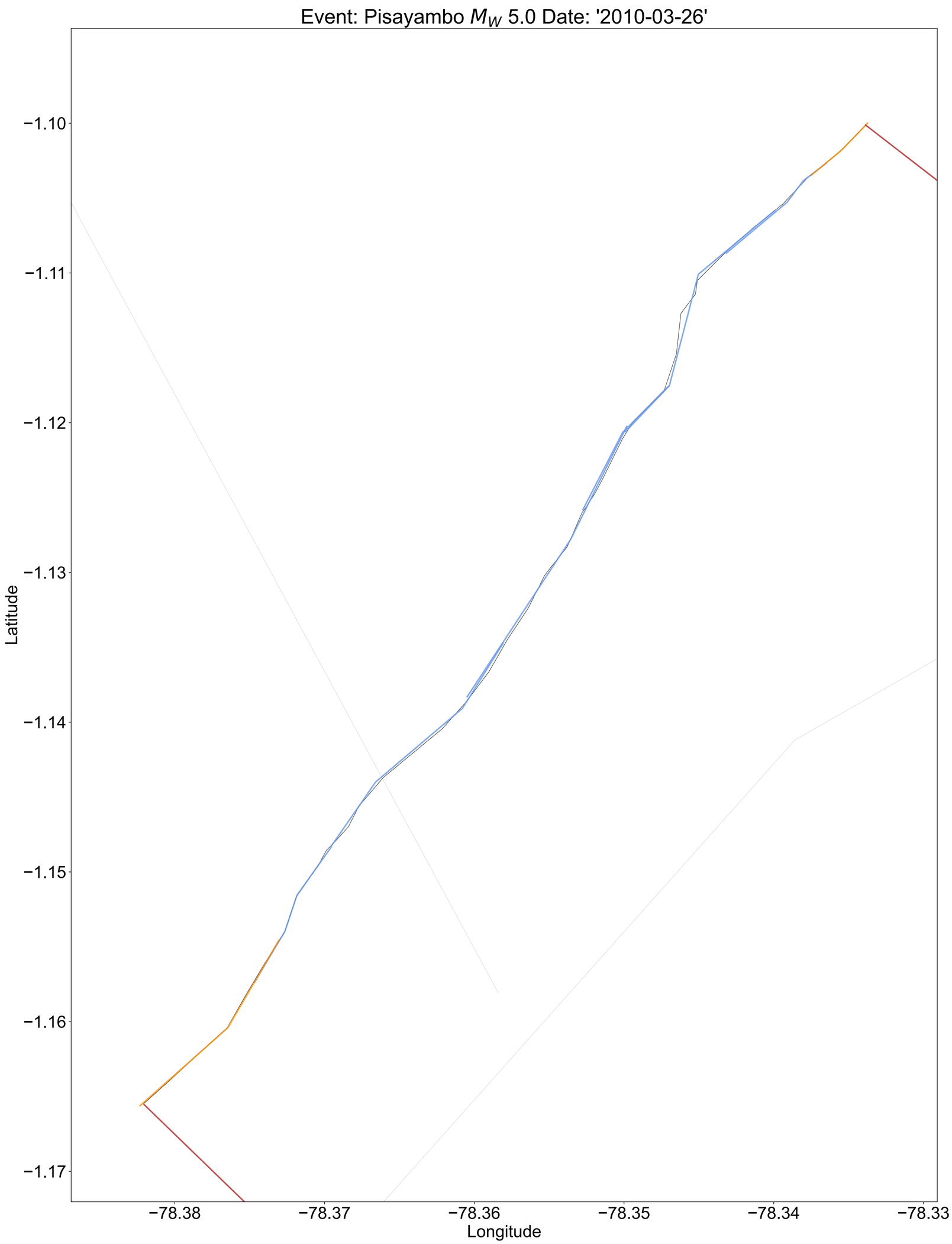
Event: Pisayambo M_W 5.0 Date: '2010-03-26'
−1.10
−1.11
−1.12
−1.13
−1.14
−1.15
−1.16
−1.17
Latitude
−78.38
−78.37
−78.36
−78.35
−78.34
−78.33
Longitude

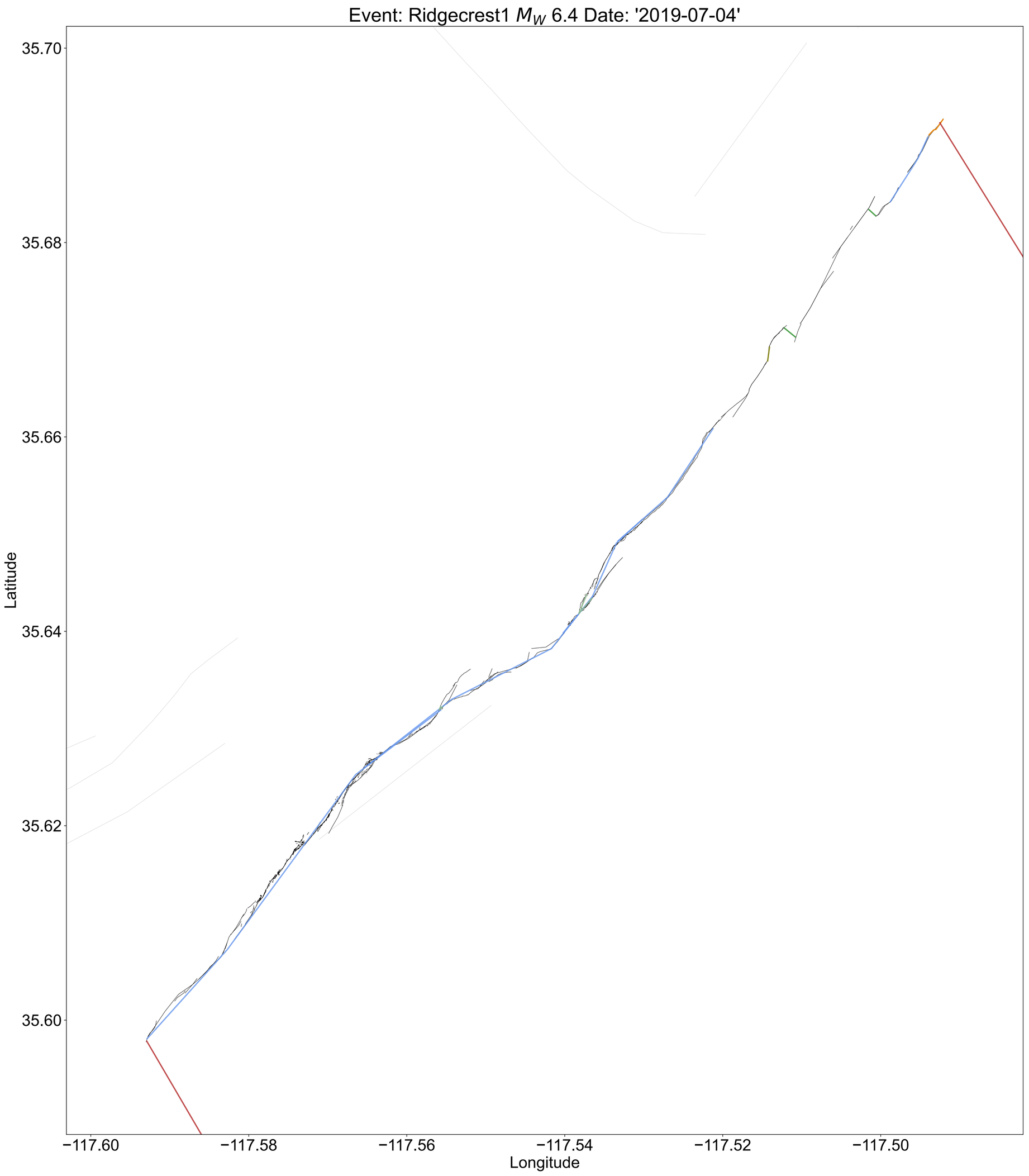
Event: Ridgecrest1 M_W 6.4 Date: '2019-07-04'
35.70
35.68
35.66
35.64
35.62
35.60
Latitude
−117.60
−117.58
−117.56
−117.54
−117.52
−117.50
Longitude

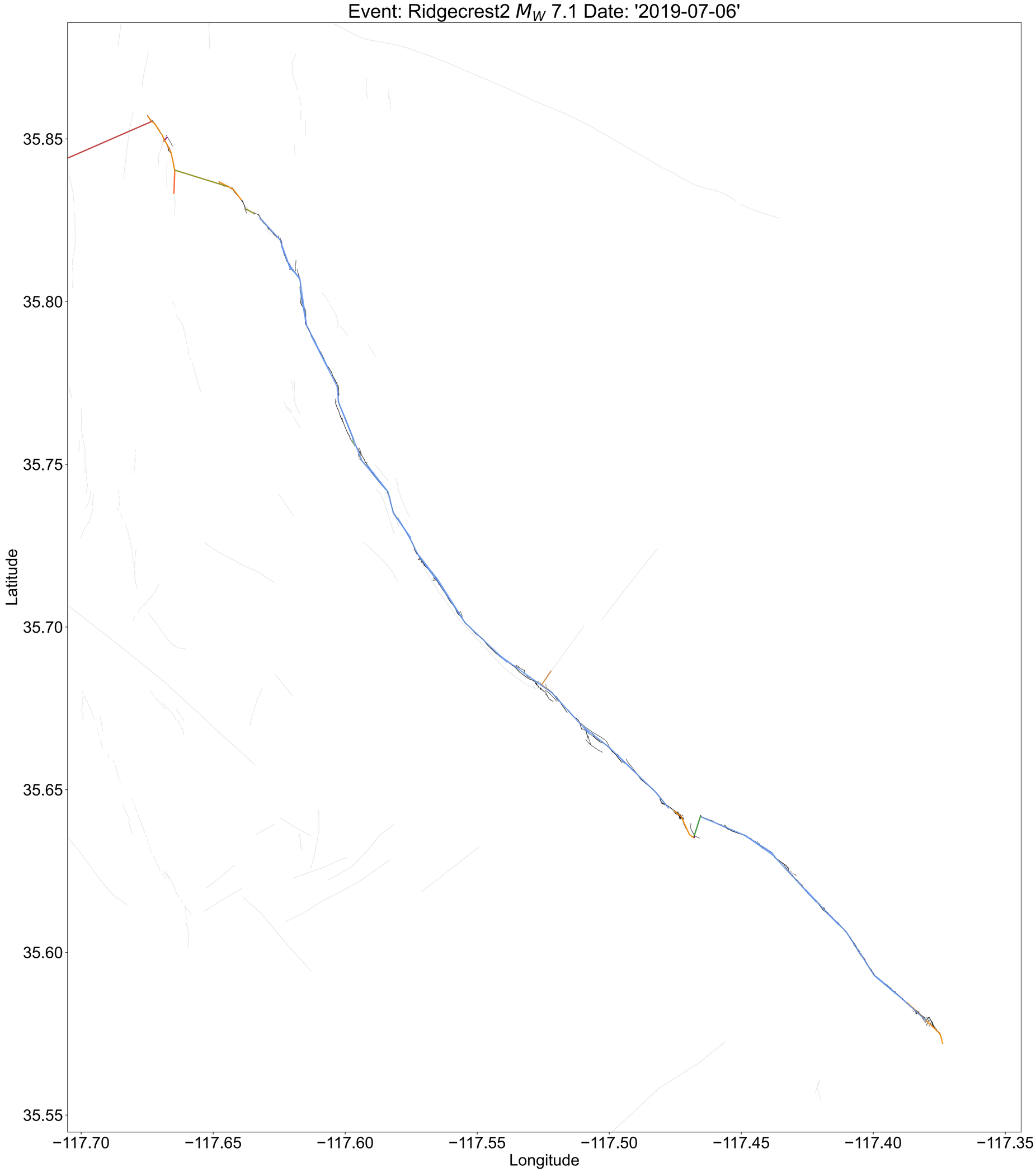
Event: Ridgecrest2 M_W 7.1 Date: '2019-07-06'
35.85
35.80
35.75
35.70
35.65
35.60
35.55
Latitude
−117.70
−117.65
−117.60
−117.55
−117.50
−117.45
−117.40
−117.35
Longitude

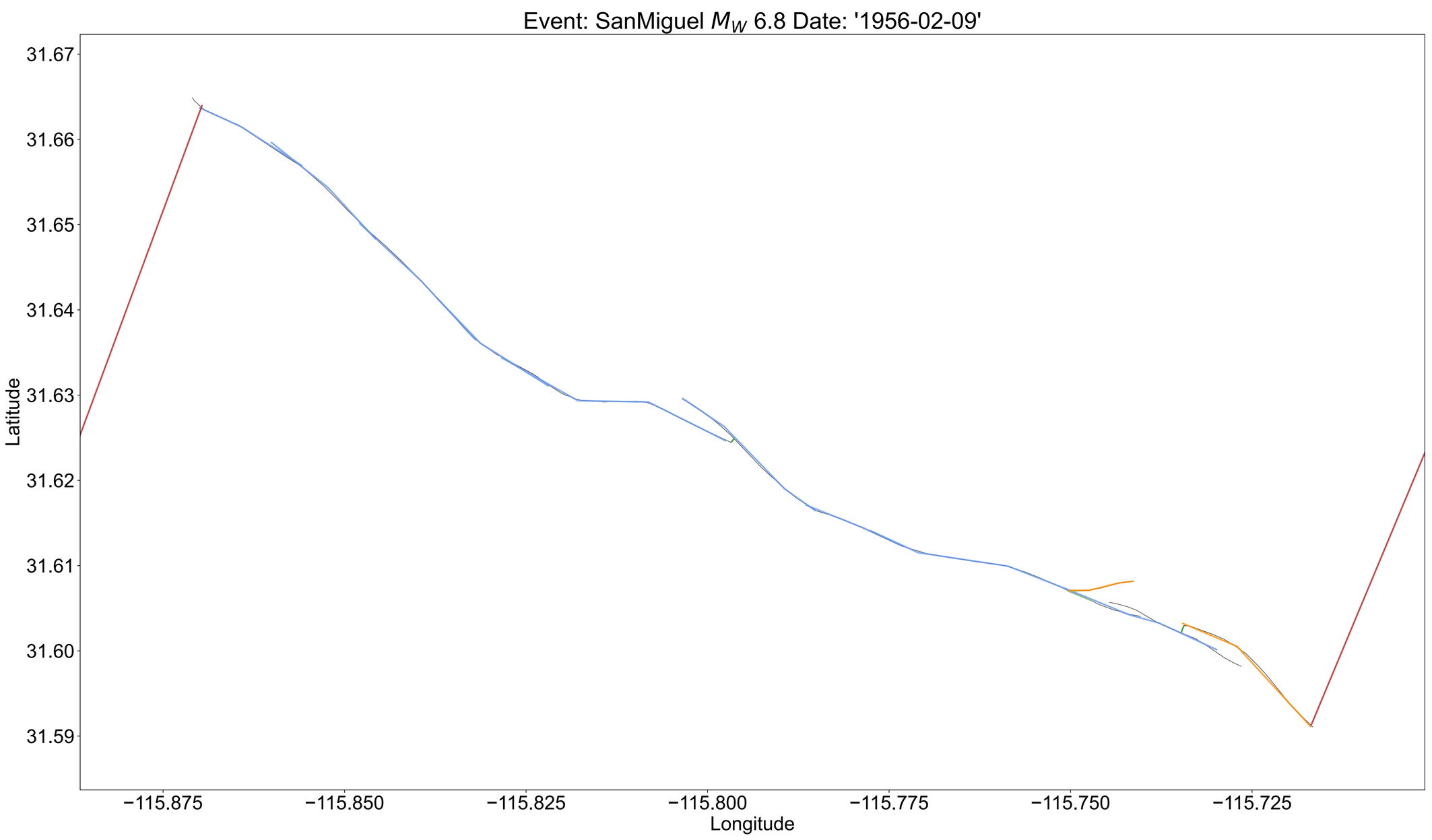
Event: SanMiguel M_W 6.8 Date: '1956-02-09'
31.67
31.66
31.65
31.64
31.63
31.62
31.61
31.60
31.59
Latitude
−115.875
−115.850
−115.825
−115.800
−115.775
−115.750
−115.725
Longitude

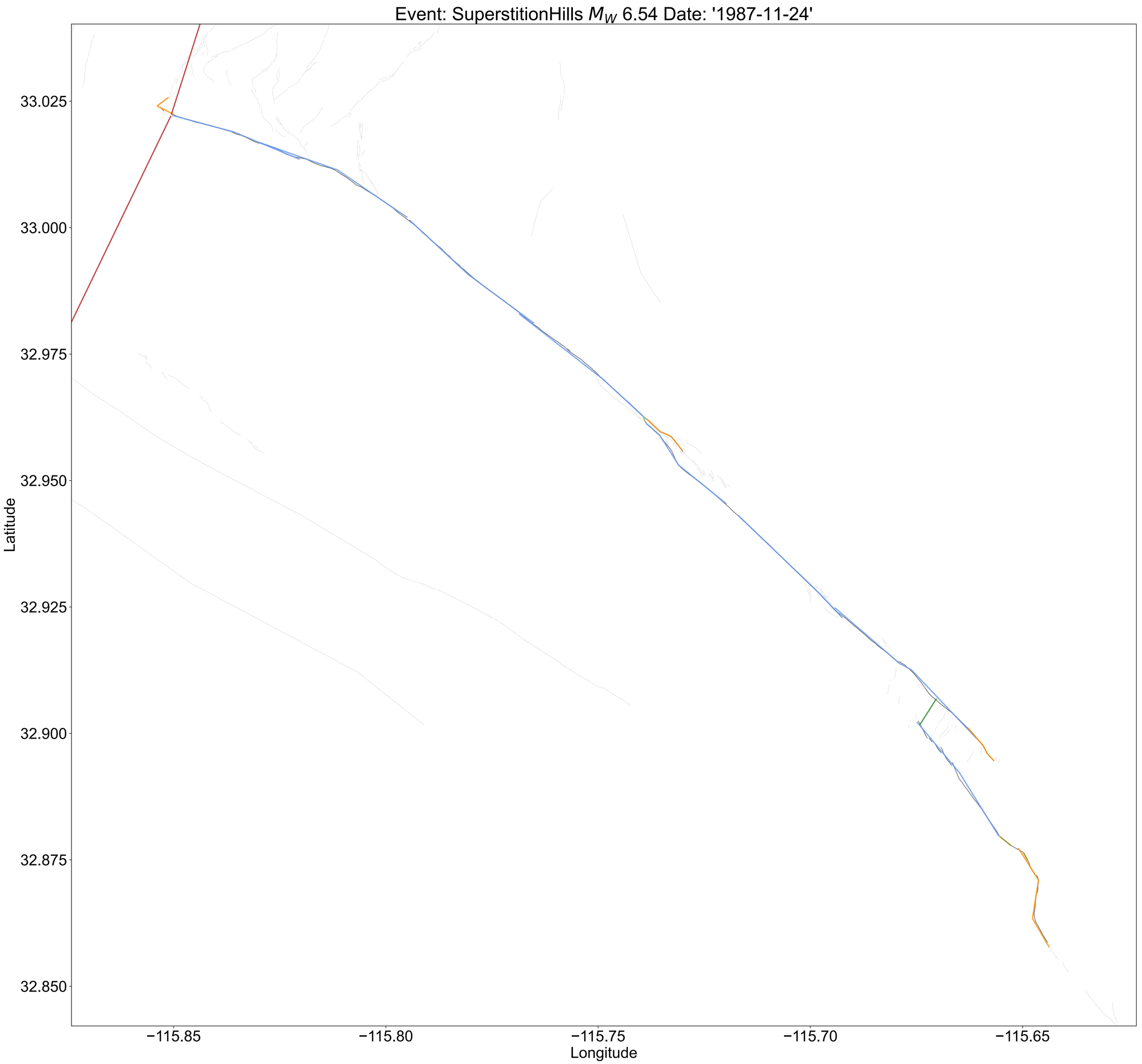
Event: SuperstitionHills M_W 6.54 Date: '1987-11-24'
33.025
33.000
32.975
32.950
32.925
32.900
32.875
32.850
Latitude
−115.85
−115.80
−115.75
−115.70
−115.65
Longitude

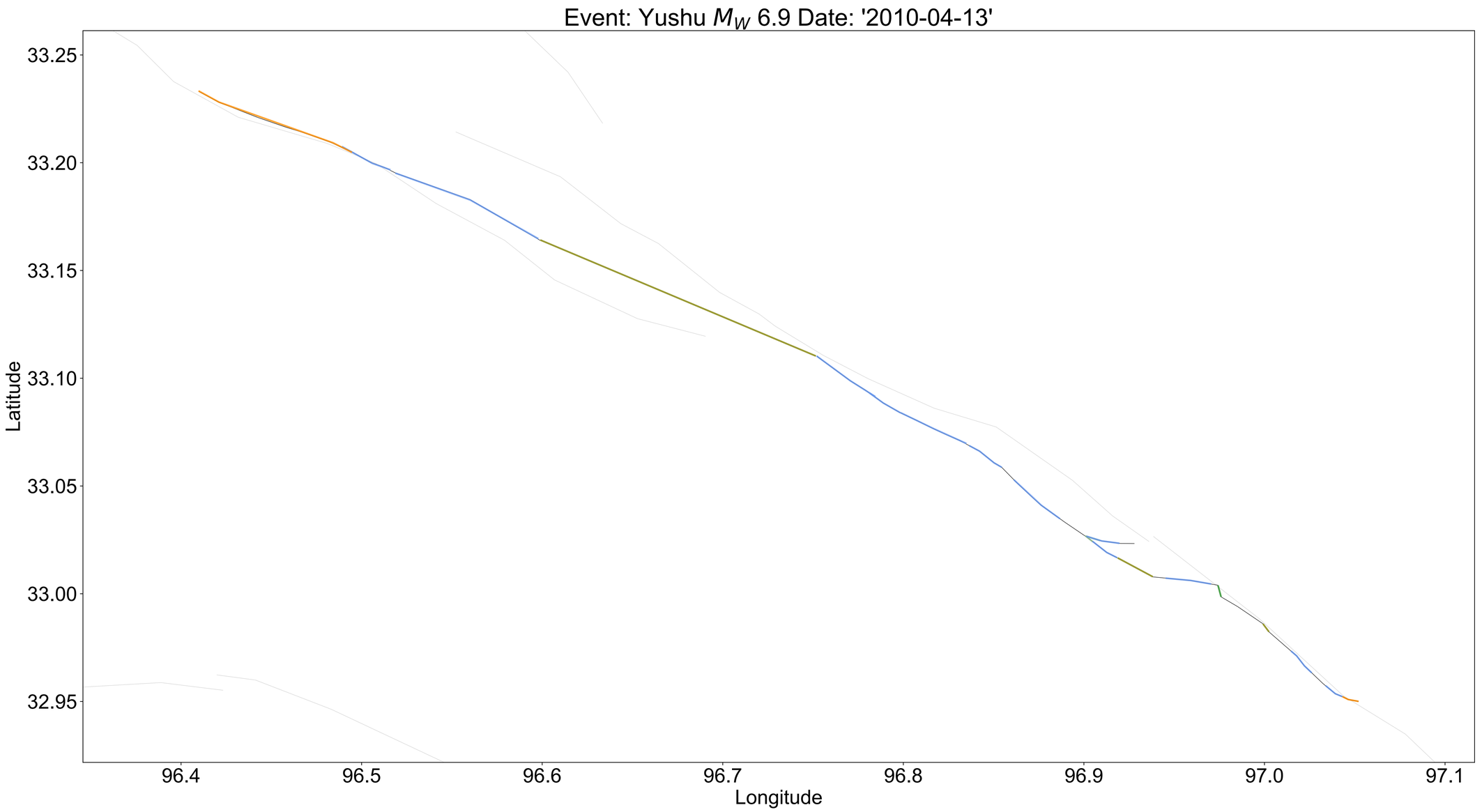
Event: Yushu M_W 6.9 Date: '2010-04-13'
Latitude
33.25
33.20
33.15
33.10
33.05
33.00
32.95
96.4
96.5
96.6
96.7
96.8
96.9
97.0
97.1
Longitude

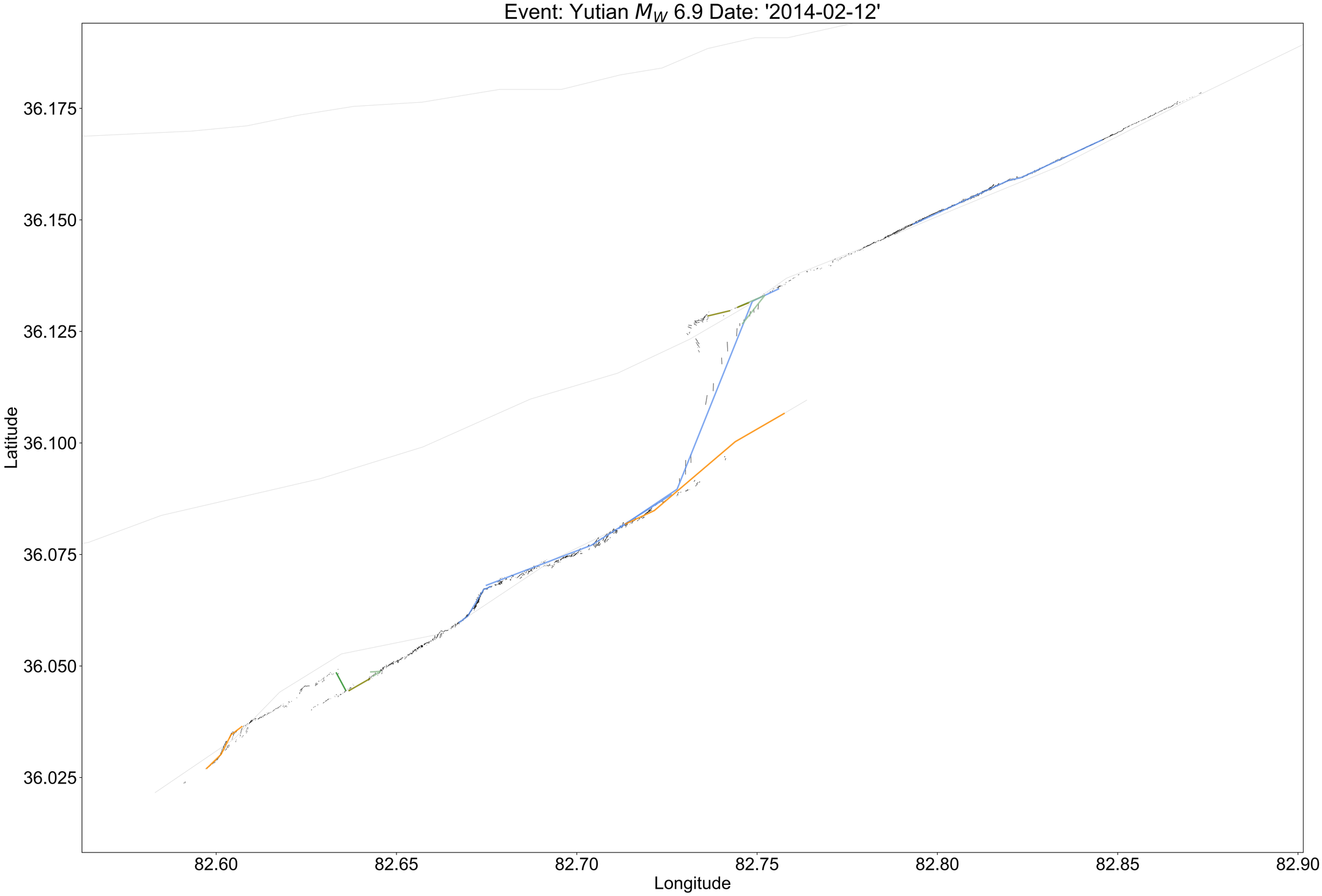
Event: Yutian M_W 6.9 Date: '2014-02-12'
Latitude
36.175
36.150
36.125
36.100
36.075
36.050
36.025
82.60
82.65
82.70
82.75
82.80
82.85
82.90
Longitude

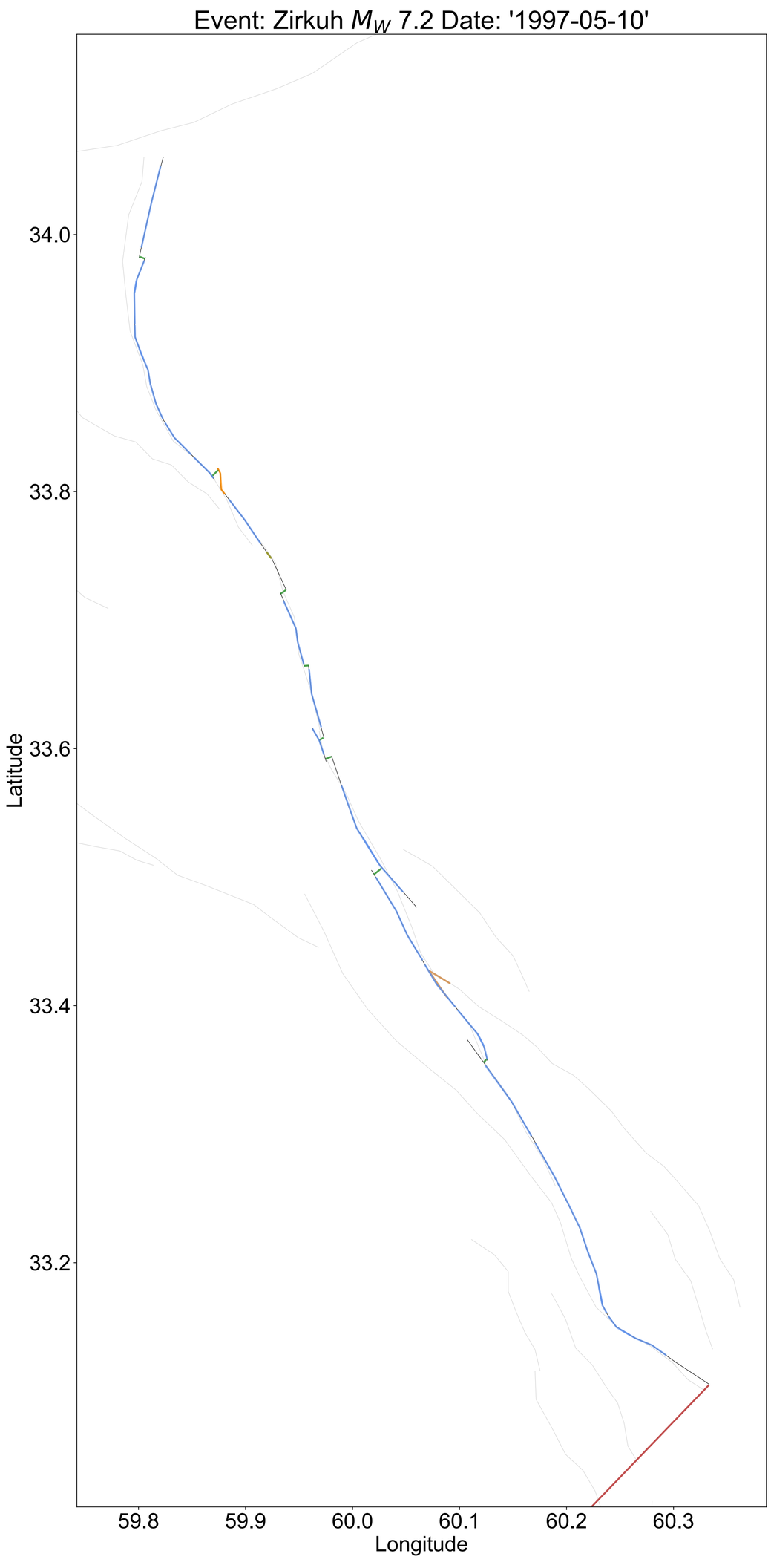
Event: Zirkuh M_W 7.2 Date: '1997-05-10'
34.0
33.8
33.6
33.4
33.2
Latitude
59.8
59.9
60.0
60.1
60.2
60.3
Longitude